Optimization of an Electrochemical Photovoltaic Cell Based on CdSe/Gel Electrolyte Junction

Maria Dochia

A Thesis
in
The Department
of
Chemistry

Presented in Partial Fulfillment of the Requirements
for the Degree of Master of Science at
Concordia University
Montreal, Quebec, Canada

April 2003

ABSTRACT

Optimization of an Electrochemical Photovoltaic Cell Based On CdSe/Gel Electrolyte Junction

Maria Dochia

In our laboratory, we developed an electrochemical photovoltaic cell (EPC) that directly converts solar energy into electricity. The cell contains a polycrystalline n-CdSe semiconducting electrode, a gel electrolyte and a transparent counter electrode (indium-tin-oxide).

In order to improve the performance of this cell, CdSe thin layers were grown by a low cost process, the liquid- metal vapor reaction. This technique has the important advantage of producing layers with a highly textured surface, leading to enhance light-harvesting capabilities. The present work involves the preparation of polycrystalline CdSe by liquid-metal vapor reaction, in which the Se vapors react with the surface of a heated Cd substrate under constant argon flow. The electrodes are characterized using: X-ray diffraction, energy dispersive analysis of x-ray, scanning electron microscopy and cyclic voltammetry. It is observed that CdSe thin films present good porosity. All the electrodes prepared in this work are of an n-type semiconductor. The gel electrolyte is composed of the redox couple CsT/T_2 (CsT is 5-mercapto-1-methyltetrazole cesium salt, T_2 is di-5-91-methyltetrazole disulfide) dissolved in a mixture of DMSO/DMF and incorporated in polyvinylidene fluoride. The use of gel electrolyte was chosen because of its large electrochemical stability domain and its ability to eliminate the photocorrosion of low band gap n-type semiconductors usually observed when using aqueous electrolytes.

ACKNOWLEDGEMENTS

I wish to express my appreciation to my supervisors, Dr. M. F. Lawrence at Concordia University (Chemistry & Biochemistry Department) and Dr. B. Marsan at UQAM (Chemistry Department) for their guidance, supervision, support and patience.

I would like to thank the members of my research committee, Dr. P. H. Bird and Dr. C. Skinner, for their cooperation and helpful suggestions.

I would like to mention and thank to Michel Preda and Raymond Mineau from the Department of Geology of l'UQAM that made possible the analysis of the X-ray diffraction patterns and also the EDAX analysis and scanning electron microscopy.

I would also like to thank my colleagues at both universities for their kindness and help.

To my son, Mircea.

CONTENTS

LIST OF FIGURES

LIST OF TABLES

CHAPTER 1

INTRODUCTION

1.1 Solar Cells

In an era where pollution is rapidly becoming a chief concern, where the burning of fossil fuels is raising the carbon dioxide content of the atmosphere and liberating sulphur, the sun with its inexhaustible power is drawing the interest of researchers and governments.[1] The sun's energy is being radiated to the earth whether it is directly used or not, and the use of photovoltaics for direct conversion of solar energy introduces no direct contamination to the environment.[2] Over the last decade, much work has gone into the development of more efficient photovoltaic energy conversion systems. Research groups across the world have been developing novel solar cell structures[3-8] that make use of new materials [9] and have significantly improved solar cells.[5]

Photovoltaic cells are devices that directly utilize the energetic photons of the incident radiation to produce electrical energy. A solar cell usually consists of a p-n junction, like that of a diode, except that the junction is of a large area; the junction lies just under the surface and collects, by virtue of its electric field, the light-generated carriers.[3] Edmond Becquerel first observed the physical phenomenon responsible for converting light to electricity - the photovoltaic (PV) effect – in 1839.[10] Chapin, Fuller and Pearson first developed the solar cell in 1954 using a diffused silicon p-n junction.[11] Since then, solar cells have provided the power for most satellites and

spacecraft launched by all nations. Solar cells have also been successfully applied in terrestrial applications, such as building power system, military installations, emergency or remote telephones, radio broadcast stations, highway dust storm and other warning signs, navigation aids for boats, ships and aircraft, solar chargeable batteries and electronic calculators.[12]

An alternative to the well-known energy conversion method involving the use of solid-state solar cells has been the method of converting solar energy with the aid of photoelectrochemical cells. The need for this alternative was dictated by the high cost of preparation of pure and perfectly crystalline semiconducting materials, and by the sophisticated technology used for the fabrication of solar cells.

1.2 Photoelectrochemical Cells (PEC)

In the past decades, the development of photoelectrochemistry as a field of science was stimulated largely by the possibility of working out a photoelectrochemical solar energy conversion method as a new, ecologically clean and inexhaustible source of energy. Photoelectrochemistry in general studies the processes involving the conversion of light energy into chemical or electrical energy in electrochemical systems. A general classification scheme for the various types of photoelectrochemical cells is presented in Figure 1.1.

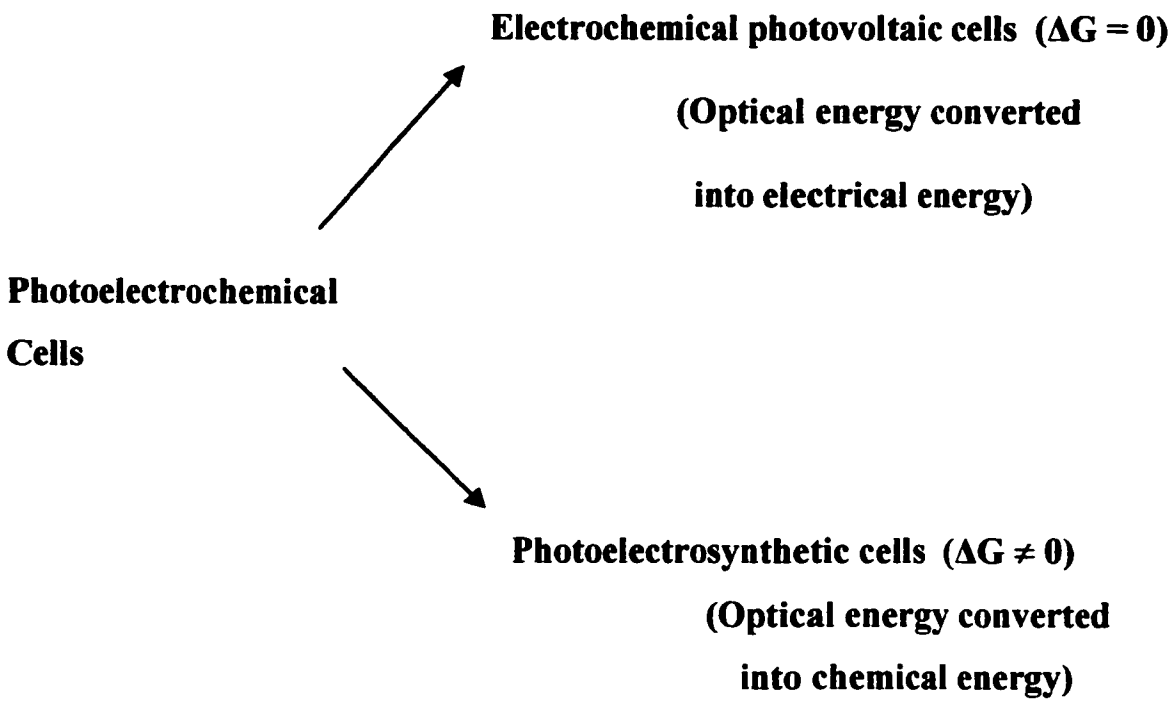

Figure 1.1 Classification of photoelectrochemical cells.

Photoelectrochemical solar cells are devices that harness light energy and convert it into electrical energy by means of an electrochemical reaction at an interface. The electrochemical photovoltaic cell (EPC) makes use of one (or two) semiconductor electrode(s) for both light absorption and separation of the photogenerated electron-hole pairs. This type of cell is the most easily constructed of all solar cells because all that needs to be done is to immerse a semiconductor electrode into an appropriate redox electrolyte and connect them through an appropriate load. Another major advantage of a semiconductor-liquid junction, over a solid-state junction, is that the high conversion efficiencies obtained with semiconductors in single crystal form can also be achieved

with less expensive polycrystalline material. This is a decisively significant factor for large-scale solar energy conversion, and it is the main reason for the large amount of work aimed at the creation of photoelectrochemical cells with polycrystalline semiconductor electrodes. Figure 1.2 shows how an EPC containing one semiconductor electrode, and a metallic counter-electrode, works. Electricity is produced when the electron-hole pairs created by illumination of the semiconductor ($h\nu \geq E_g$) are separated in the space charge layer near the semiconductor/electrolyte interface, with the majority carriers being driven into the bulk of the semiconductor while the minority carriers are driven to the semiconductor/electrolyte interface. The minority carriers (holes in an n-type material or electrons in a p-type material) oxidize or reduce the redox species in the electrolyte while the majority carriers pass through the external circuit containing a load and accomplish the opposite reaction at the counter-electrode. An important problem arises with these cells because the minority carriers are usually highly reactive and so the semiconductor itself may undergo an oxidation or a reduction reaction with the photogenerated minority carriers, e.g.:

$$n\text{-}CdSe + 2h^+ \longrightarrow Cd^{2+} + Se \qquad (1.1)$$

if n-type CdSe is used as the semiconductor material in an aqueous electrolyte. This is known as photocorrosion, a process that remains one of the major obstacles to the development of efficient and stable photoelectrochemical solar cells.[13,14]

Efficient solar cells require semiconducting materials with band gaps of 1.3±0.3 eV. In general, band gap and stability are correlated: the lesser the band gap the lesser

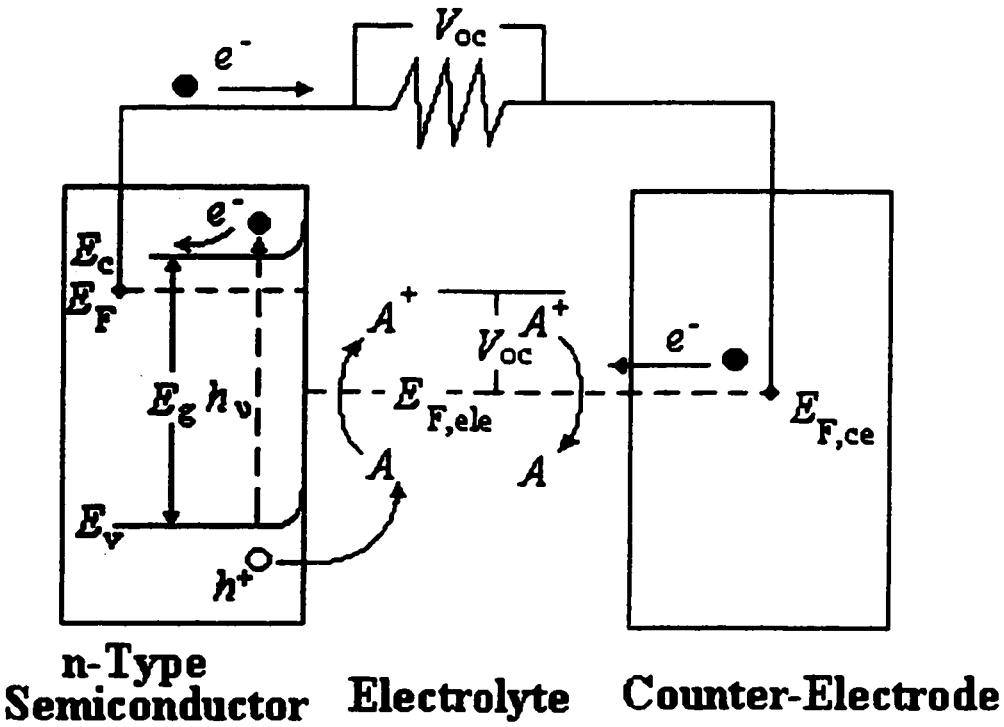

E_V : Valence band energy
E_C : Conduction band energy
E_g : Band gap energy
E_F : Fermi level of the semiconductor
$E_{F,ele}$: Fermi level of electrolyte
$E_{F,ce}$: Fermi level of counter-electrode
V_{oc} : Open-circuit potential (photo-voltage)

Fig. 1.2 Energy diagram of an electrochemical photovoltaic cell. [73]

the photoelectrochemical stability.[15,16] However, stability can be attained by making a suitable choice of the solution redox couple or solvent, and by modification of the electrode surface. In the literature, most of the electrochemical photovoltaic cells that have been studied use an aqueous electrolyte[17-21] and systems giving good conversion efficiency are generally unstable under sustained illumination.[19] Table 1.1 lists some efficient EPC's that have been constructed using single crystal semiconductor materials.

Table 1.1 Efficient electrochemical photovoltaic cells constructed from single crystal semiconductor materials.

Semiconductor	Redox Electrolyte	η^a (%)	$(10^3$ C·cm $^{-2})^b$	Reference
n-GaAs	1M K_2Se, 0.01M K_2Se_2, 1M KOH	12.0	35	(22, 23)
n-WSe_2	1M KI, 0.01 M KI_3	10.2	400	(24, 25)
n-$MoSe_2$	1M KI, 0.01M KI_3	9.4	50	(24)
n-CdSe	1M Na_2S_2, 1M NaOH	7.5	20	(26)

[a] sunlight energy conversion efficiency
[b] the amount of charge that has been passed through the cell

In order to solve the photocorrosion problem several scientists have considered the use of solid polymer electrolytes as an alternative.[27-33, 68] Such electrolytes could eliminate photocorrosion due to their low solvation energy for ions. Moreover, they

enable the fabrication of very thin, all-solid-state cells, and thus there is no leakage and very little absorption of visible light by the electrolyte. Poly (ethylene oxide) (PEO), $[-CH_2-CH_2-O-]_n$, for example, has already been used in high energy density lithium batteries and electrochromic devices. Skotheim et al.[27-29] were the first to use PEO in contact with a n-Si single crystal in a EPC. Vijh and Marsan[31] were the first to use a solid polymer electrolyte in contact with a polycrystalline semiconducting electrode, n-CdSe/modified PEO-M_2S/xS, where M = Li, Na and K; x = 1, 3, 5, and 7. Recently, Philias and Marsan[33, 68] investigated the cell n-CdSe//high molecular weight PEO-based copolymer (modified $PEO)_{12}$ – CsT/0.1 T_2//ITO where CsT stands for 5-mercapto-1 methyltetrazole cesium salt, T_2 for di-5-(1-methyltetrazole) disulfide and ITO for indium-tin-oxide conducting glass. These EPCs demonstrated very stable short-circuit current densities and open-circuit potentials when they were illuminated. However, the electrical resistance of the polymer electrolytes (therefore of the cells) was high and the energy conversion efficiency was low. At 100mW/cm^2 illumination (surface area: 1.2 cm^2), the cell yields a current density of 650 μA/cm^2, an open-circuit potential of 0.54 V, a fill factor of 0.32 and an energy conversion efficiency of 0.11%. The cells also needed to be operated above room temperature (~50^{0}C).

Recently, researchers have been paying more attention to the study of another type of electrolyte, the gel electrolyte, for application in electrochemical devices.[34-38] A gel electrolyte is a liquid electrolyte incorporated in an almost non-interacting polymeric matrix. It is a three-component system, including a salt (redox couple), a low molecular weight aprotic polar solvent (or mixture of solvents), and a polymer. The properties of gel electrolytes lie between those of liquid and solid polymer electrolytes

and, in general, they help to lower the rate of corrosion and improve the stability of the EPCs with respect to those based on aqueous electrolytes. Since diffusion of the redox couple in a gel is better than that in a solid polymer, the conductivity of the system is expected to be higher ($\sim 10^{-3} S \cdot cm^{-1}$ at $25^0 C$). Because the energy conversion efficiency, in the case of solid polymer electrolytes, is strongly related to the conductivity of the electrolyte,[31] the PEC would have a greater efficiency than that of a cell using a solid-polymer electrolyte. Other important advantages of liquid junction cells, over solid state devices, are that the light is absorbed right at the interface, so that the photogenerated carriers move only a short distance before they react, thus diminishing the loss due to the recombination at the surface, and the possibility of choosing different redox couples in the electrolyte that permit the optimization of the characteristics of the PEC.

In examining the processes occurring at the semiconductor/electrolyte interface, it is important to discuss some of the electrical and optical characteristics of the semiconductors before considering the photoelectrochemical phenomena at the interface.

1.3 Theory of Semiconductors

The energy band diagram, which determines the optical and electrical characteristics of a semiconductor, is shown in Figure 1.3. The energy is given by the vertical axis; E_V and E_C are respectively the level of the top of the valence band (upper of the filled orbitals at 0 K) and that of the bottom of the conduction band (the next empty band at 0 K). The valence band is derived from the overlap of filled valence orbitals of the individual atoms of the crystal, and the conduction band from the overlap of empty higher orbitals of the

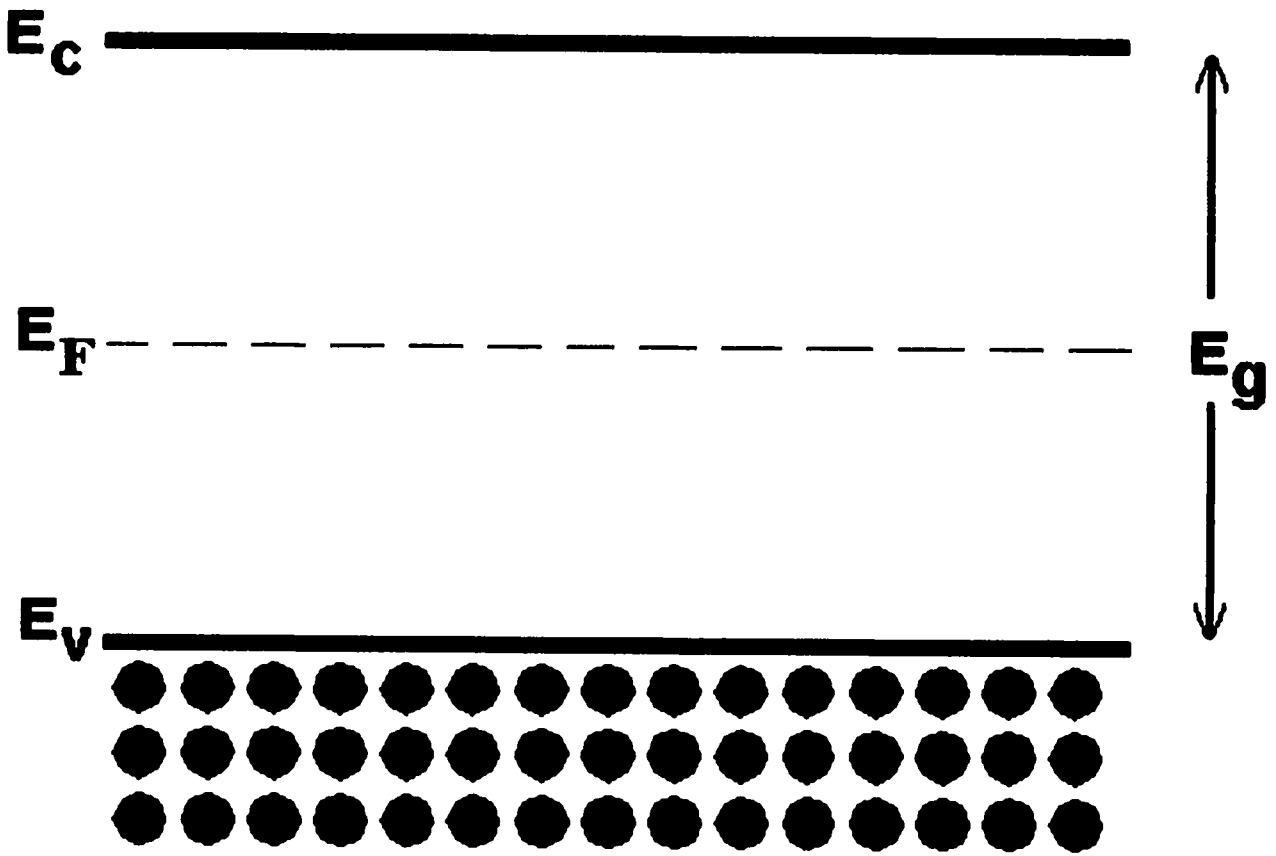

Fig. 1.3 The intrinsic semiconductor energy level diagram. E_C = lowest level of the conduction band (empty at 0 K); E_V = highest level of the valence band (filled at 0 K); E_g = band gap energy; E_F = Fermi level; ● : electrons.

atoms involved. Each of these bands is composed of upper and lower levels that arise owing to the symmetrical and antisymmetrical linear combination of atomic orbitals (bonding and antibonding molecular orbitals, respectively). The difference $E_C - E_V = E_g$ is the width of the forbidden band called also the band gap energy.

A perfect semiconductor crystal with no impurities or lattice defects is called an intrinsic semiconductor. Figure 1.3 represents such a semiconductor. At 0 K, an intrinsic semiconductor is an insulator, because its valence band is completely occupied and its conduction band totally empty. At a temperature much higher than 0 K, there are some electrons with thermal energy (kT) larger than E_g. This energy is sufficient for transferring electrons from the valence band into the conduction band, and in this case, positive holes (h^+) remain in the valence band: $|e^-| = |h^+| \approx 10^{13} - 10^{16}$ cm^{-3} compared to ~ 10^{22} cm^{-3} in a metal. Both the electrons in the conduction band and holes in the valence band are involved in the transmission of the electrical current through the semiconductor. An extrinsic semiconductor is one in which additional carriers are present in the conduction or the valence band. In this case, mobile carriers appear due to the ionization of impurity atoms referred to as:

-Donors: adding electron donors to an intrinsic semiconductor introduces filled energy levels between the Fermi level and the conduction band, whose ionization gives additional electrons in the conduction band. This is the n-type semiconductor for which $|e^-| >> |h^+|$.

-Acceptors: adding electron acceptors to an intrinsic semiconductor introduces empty energy levels between the Fermi level and the valence band, whose ionization gives

additional holes in the valence band. This is called the p-type semiconductor for which $|h^+| >> |e^-|$.

Donor impurities, in n-type semiconductors, have energy levels, E_D, a few kT below the conduction band (Figure 1.4a) and, electron acceptors in p-type semiconductors have energy levels, E_A, a few kT above the valence band (Figure 1.4b); this is why these impurities get completely ionized even at room temperature. Electrons can be promoted from the valence band to the conduction band upon absorption of light. A necessary condition for absorption is that the incident photon energy equals or exceeds the band gap energy ($h\nu \geq E_g$). A photon with a greater energy than E_g contributes an energy E_g to the cell's electrical output, and the energy in excess of E_g is converted into heat. This is the primary event in the conversion of sunlight to usable forms of energy.

1.4 Fermi Level

The equilibrium behaviour of the electron system of a semiconductor is described by the electrochemical potential of the electrons known as the Fermi level, E_F. The Fermi level corresponds to the energy (E) of the level for which the probability of occupancy by electrons, P(E), is exactly 0.5. At $T > 0$ K, there is no sharp distinction between occupied and unoccupied orbitals in a bond because electrons can be excited by thermal motion of the atoms.

The probability of occupancy increases with energy below the Fermi level and decreases with energy above the Fermi level in accordance with the Fermi-Dirac distribution function[89]:

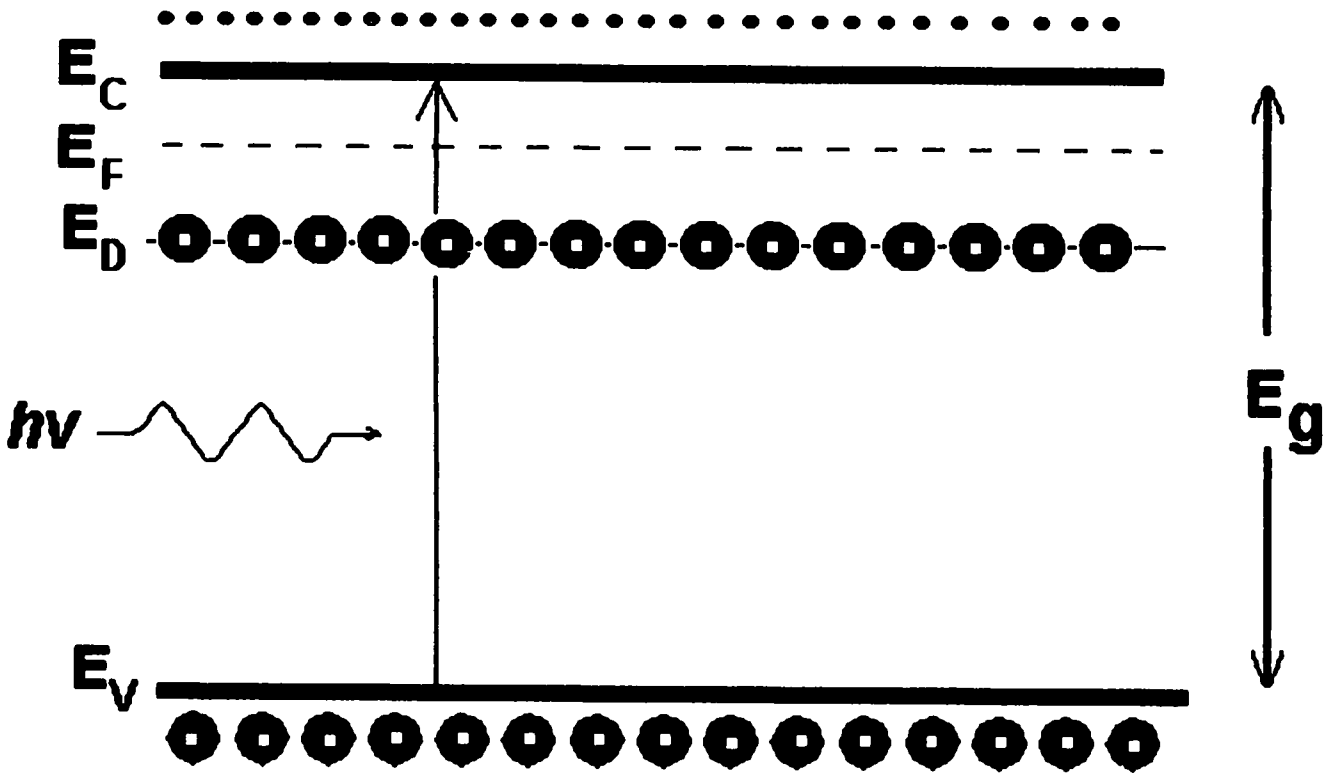

Fig. 1.4 a) The n-type semiconductor energy level diagram. E_D = Donor energy

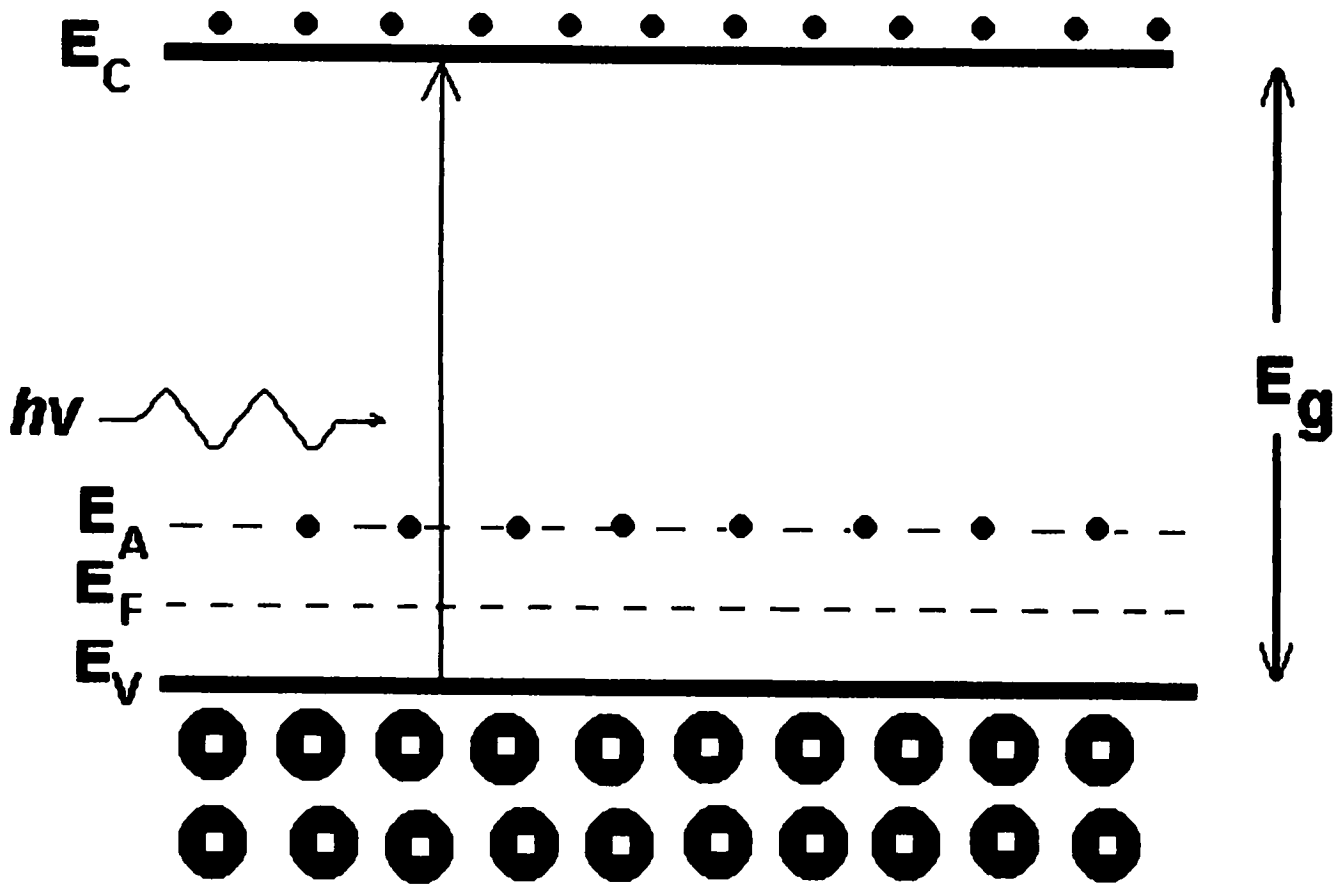

Fig. 1.4 b) The p-type semiconductor energy level diagram. E_A = Acceptor energy levels

$$P(E) = \frac{1}{1 + \exp \frac{E - E_F}{kT}} \qquad (1.2)$$

where k is the Boltzmanns' constant (1.38×10^{-23} J K^{-1}) and T is the absolute temperature. For energies well above the Fermi energy, the 1 in the denominator can be neglected,

$$P(E) \simeq e^{-(E - E_F) / kT} \qquad (1.3)$$

and the population now resembles a Boltzmann distribution, decaying exponentially with increasing energy.

In a semiconductor, the Fermi level is located inside the band gap. For an intrinsic semiconductor, E_F occurs midway between the conduction and valence band edges (Figure 1.3). Doping shifts the Fermi level with respect to the band edges. N-type doping (electron donor impurities) results in shift of E_F toward E_C midway between E_D and E_C at 0 K (Figure 1.4a). The shift is consistent with the fact that the probability of occupancy of the energy level E_D is 1 at 0 K; thus, the energy at which the probability equals ½ lies between E_D and E_C. Likewise, p-type doping (electron acceptor impurities) shifts E_F between E_V and E_A at 0 K (Fig. 1.4b); the probability of occupancy of the energy level E_A is 0. It is important to note that the temperature has an effect on the position of E_F: the Fermi level is shifted slowly toward the value expected for an intrinsic semiconductor [$E_F = (E_C + E_V)/ 2$] as T is raised.[90]

1.5 Semiconductor – Electrolyte Junction

In liquid junction photovoltaic cells, the aim is the production of an electrical current flow and a voltage without net changes occurring in either the electrolyte solution or the electrode materials. These cells, which are the photoelectrochemical equivalent of solid-state solar cells, utilize a single redox couple in the solution.

When a semiconductor is immersed in a solution containing a redox couple, charge transfer occurs at the interface because of the difference in the tendency of the the two phases to lose electrons (that is, difference in electron affinity or electrochemical potential of the two phases). The net result is the formation of an interphase between the semiconductor and the electrolyte. The structure of the interphase is divided into three regions: the diffuse layer (Gouy - Chapman) and the Helmholtz layer in the solution side, and the space charge region (diffuse layer) in the semiconductor side. The Gouy - Chapman layer is the thickness of electrolyte where the ion concentration deviates from the bulk electrolyte values. The Helmholtz layer is the region between the electrode surface and the plane of closest approach for solvated ions (taking into account the contact adsorbed ions). The formation of a space charge region, called also the depletion layer, within a semiconductor is a consequence of the mismatch of the Fermi level of the semiconductor (E_F) and the Fermi level of the electrolyte ($E_{F,ele}$). If the Fermi level of an n-type semiconductor is above the Fermi level of the electrolyte, than equilibration of the two Fermi levels occurs by transfer of electrons from the semiconductor to the electrolyte. As a result, the conduction and valence band edges are bent upwards, establishing a potential barrier against further electron transfer into the

electrolyte (Figure 1.5). The electric field thus created at the interface enables spatial separation of photogenerated electron-hole pairs, therefore producing electric current and a voltage. At equilibrium, the band bending is energetically equal to the initial difference in the Fermi levels of semiconductor and electrolyte. Application of the equilibration concept to the semiconductor / electrolyte interface requires the definition of the Fermi level in an electrolyte. For liquid electrolytes, the chemical potential of electrons is determined by the redox potential of the couple present in the electrolyte and is identified with the equilibrium potential (V_{rdx}) according to the following equations:

(1.4)

$$\mathbf{OX + ne^- \Leftrightarrow RED}$$

$$V_{rdx} = V^0 - \frac{RT}{nF} \ln \frac{[RED]}{[OX]} \tag{1.5}$$

$$E_{F,ele} = -(eV_{rdx} + 4.5\ eV) \tag{1.6}$$

where OX is the oxidized form and RED the reduced form of the redox couple, n is the number of electrons transferred per molecule, e is the electron charge and V^0 is the standard potential. $E_{F,ele}$ corresponds to the "Fermi level" of the electrolyte solution expressed on the absolute energy scale, whose reference point is defined below. The solution "Fermi level" arises from the concept that OX and RED molecules, in an electrolyte, form a set of electron-energy levels, of which the OX molecules represent the unoccupied levels and the RED molecules the occupied ones. For semiconductors, the Fermi level gives the chemical potential of electrons. By convention, the Fermi level

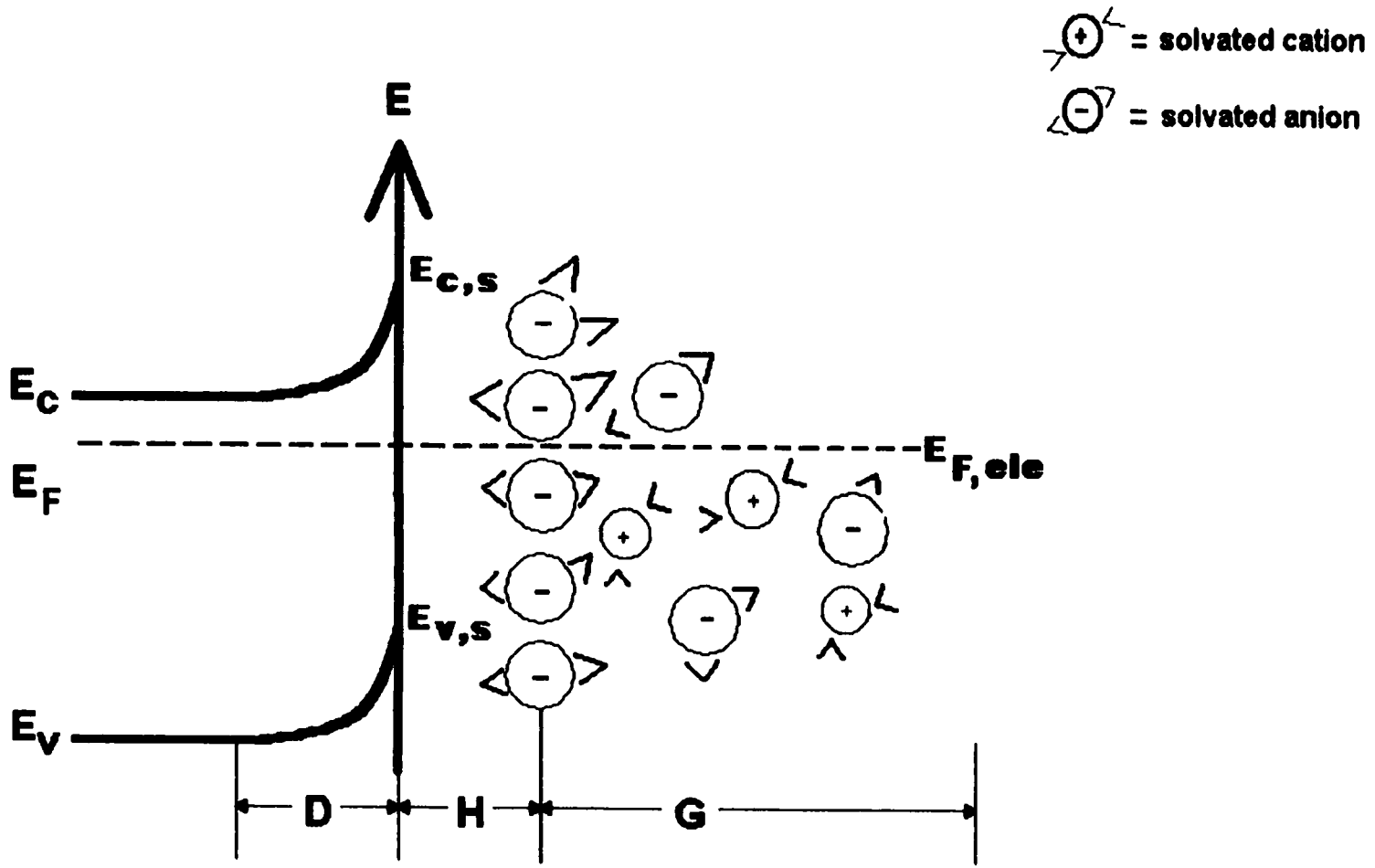

Fig. 1.5 Equilibrium energy level diagram for an n-type semiconductor – electrolyte junction; H = Helmholtz layer; G = Gouy – Chapman layer; D = depletion layer; $E_{C,S}$ = lowest level of the conduction band at the surface; $E_{V,S}$ = highest level of the valence band at the surface; E_F = Fermi level of the semiconductor; $E_{F,ele}$ = Fermi level of the electrolyte;

is defined relative to the energy of an electron in vacuum (absolute energy scale) while the electrochemical potentials are defined relative to the standard hydrogen electrode (Figure 1.6). The two scales are related by the theoretical value for the Fermi level of the SHE[39]:

$$E_{F,H^+/H_2} = -4.5 \text{ eV} \qquad (1.7)$$

At equilibrium, the Fermi level in the redox electrolyte and in the semiconductor coincide (Figure 1.5), and electron transfer occurs between occupied surface semiconductor band energy levels and empty energy levels of the oxidized species, or occupied energy levels of the reduced species and empty surface energy levels of the semiconductor.

1.6 The Effect of Applied Potential

In the electrochemical cell, all changes in the potential applied to the semiconductor working electrode affect the potential drop across the semiconductor / electrolyte interface. As mentioned previously, there are three regions of varying electrical potential at a fixed applied potential[40] (Figure 1.5): the Gouy – Chapman diffuse layer, the Helmholtz layer and the depletion layer within the semiconductor electrode in which the electrical potential varies from the surface to the bulk.

The potential changes smoothly across the width of the depletion layer. Because an electron at a band edge exhibits different energies in regions of varying electrical potential, the band edges bend accordingly. The band bending can be downwards (n-type semiconductor), with E_C and E_V higher at the surface than in the bulk, or upwards

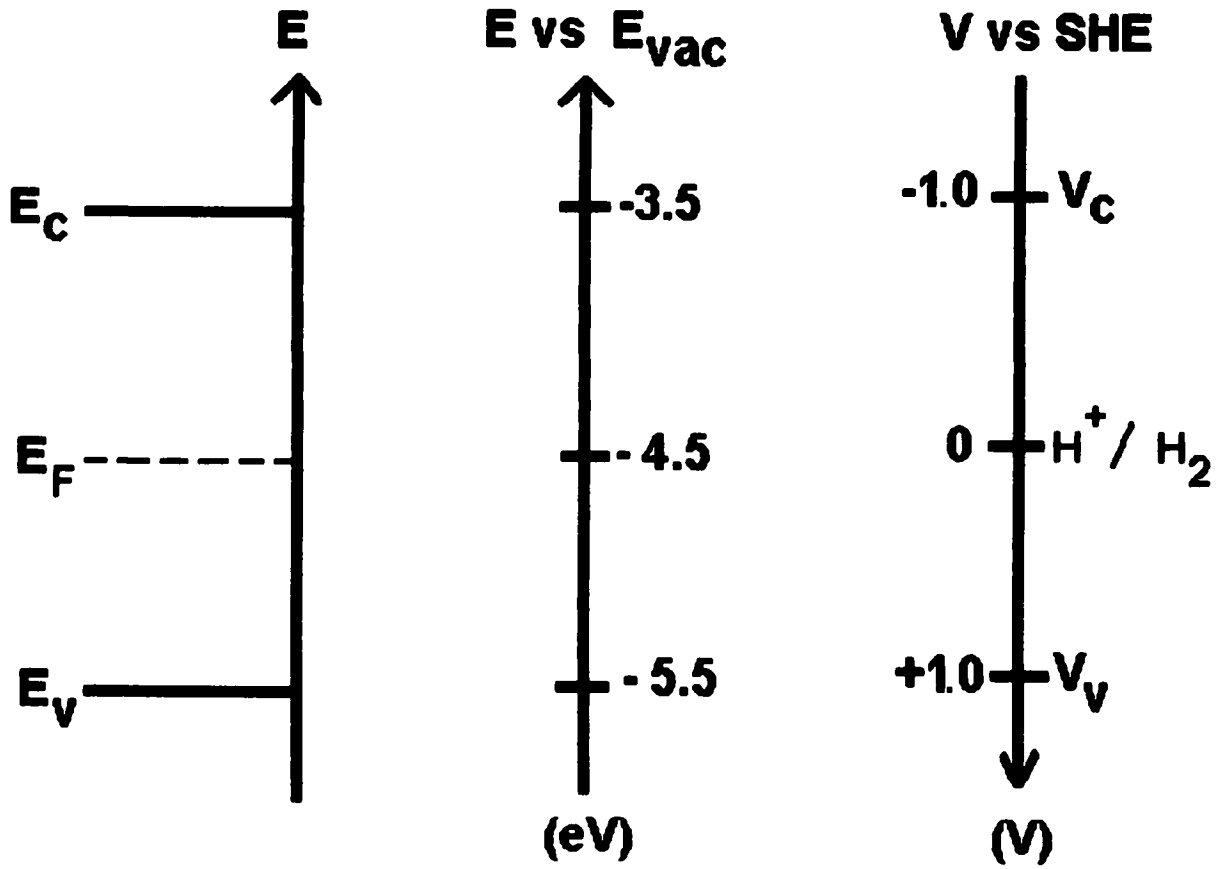

Fig. 1.6 The absolute energy and electrochemical potential scales for an intrinsic semiconductor with $E_g = 2.0$ eV.

(p-type semiconductor). The magnitude of the band bending is equal to the total potential drop across the depletion layer, $E_{C,s} - E_{C,b}$, where s and b subscripts refer to the surface and the bulk, respectively.

The Fermi level stays at constant energy from the bulk to the surface, so the position of Fermi level relative to the band edges changes at the surface. And this is the reason that the hole (p-type) and electron (n-type) concentrations are perturbed at the surface relative to the bulk. The concentration of charge carriers is described by the following expressions, derived from the Boltzmann's distribution factor (eq. 1.3 with $P(E) = [e^-] / N_C$ or $[h^+] / N_V$):

$$[e^-] = N_C \exp[-(E_C - E_F)/kT] \quad \text{with } E_C > E_F \tag{1.8}$$

$$[h^+] = N_V \exp[-(E_F - E_V)/kT] \quad \text{with } E_F > E_V \tag{1.9}$$

where $[e^-]$ and $[h^+]$ are the electrons and hole densities, respectively, and N_C and N_V are the effective density of energy levels at the conduction band edge and valence band edge, respectively (~2.5×10^{19} cm^{-3} at 25^0C). For the case of downwards band bending shown in Figure 1.5 (n-type semiconductor), electrons are depleted ($E_C - E_F$ larger at the surface) and for the case of upwards band banding (p-type semiconductor) holes are depleted ($E_F - E_V$ larger at the surface).

When the negative bias applied to an n-type semiconductor is increased, the surface barrier height (band bending) is decreased and vanishes as the flat band potential, V_{fb}, is reached (see Figure 1.7d). Injection of additional electrons (majority

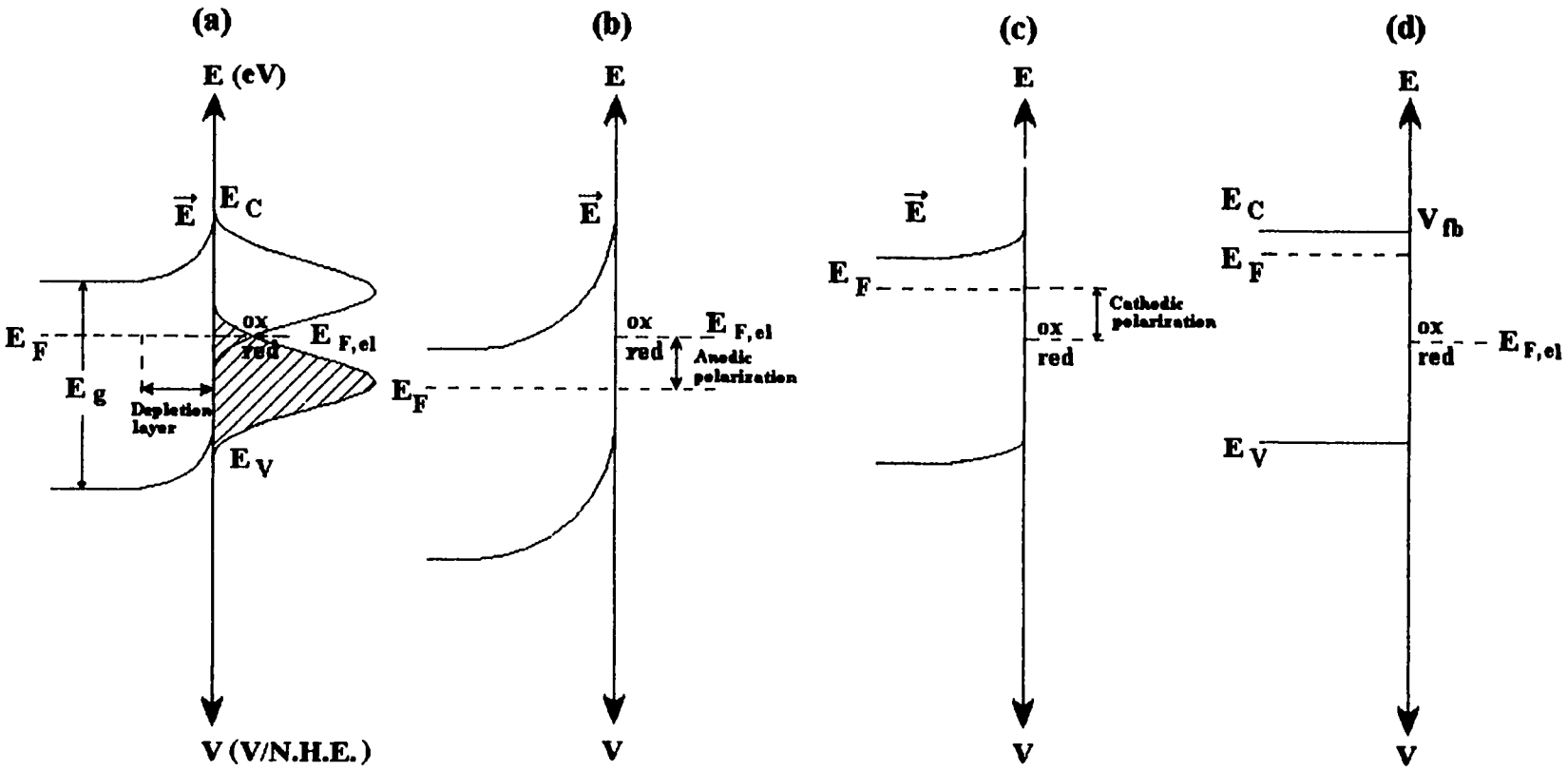

Fig 1.7 Energy diagram of n-type semiconductor/ electrolyte junction: (a) equilibrium; (b) anodic polarization; (c) cathodic polarization; (d) at the flat band potential.

charge carriers) creates an accumulation region and a charge transfer leading to reduction of the oxidised species in the electrolyte; the result is a cathodic current. In the dark, the anodic current, which is the current due to minority charge carriers (holes), is very weak because the concentration of holes in the semiconductor under these conditions is many orders of magnitude smaller (Figure 1.7b). At more positive potentials, oxidation of the reduced species in the electrolyte via the conduction band is observed through charge transfer across the barrier via a tunnelling effect.

1.7 The Effect of Illumination

The semiconductor/electrolyte junction determines the photoelectrochemical behaviour of the semiconductor and is responsible for the conversion of light to electricity. An electron can be promoted from the valence band to the conduction band upon the absorption of a photon. A necessary condition is that the photon energy exceeds the band gap energy ($h\nu \geq E_g$) of the semiconductor. Defining λ_g

$$\lambda_g\,(\text{nm}) = \frac{1240}{E_g\,(\text{eV})} \qquad (1.10)$$

according to equation 1.10, wavelengths greater than λ_g are not absorbed by the semiconductor. At wavelengths shorter than λ_g, photons are absorbed within a short distance of the semiconductor surface. The semiconductor thus exhibits a threshold response to light.

The dependence of photocurrent or semiconductor absorption coefficient on excitation wavelength provides information about the band gap energy and the nature of the optical transition (direct or indirect). In a direct band gap semiconductor, a photon with energy just equal to the direct band gap energy is absorbed with the creation of a hole and an electron. In the case of indirect band gap, the transition of an electron from the valence to the conduction band is accompanied by the emission of a phonon (quantized lattice vibration) of energy q and therefore requires less energy according to equation 1.11:

$$E_g = h\nu - q \tag{1.11}$$

When an n-type semiconductor electrode is biased sufficiently positive to the flat band potential (V_{fb}, the potential at which there is no band bending), the dark currents are very low due to the blocking effect of the depletion layer. Upon irradiation of the semiconductor through the electrolyte ($\lambda < \lambda_g$), electron-hole pairs are generated. Charge carriers generated in the space charge layer move in opposite directions as of result of the electric field. If no recombination occurs, the majority carriers (e^-) migrate to the bulk and the minority carriers (h^+) to the surface (Figure 1.8). For n-type semiconductor electrodes, in an ideal case, the holes react at the interface exclusively with the electrolyte, oxidizing the electron donors (Red) of the redox system. The electrons in the conduction band flow via an external circuit to the other electrode, the counter electrode, where the reduction takes place at its Fermi level ($E_{F,M}$). In the electrochemical photovoltaic cell, the two electrode reactions are inverse to each other:

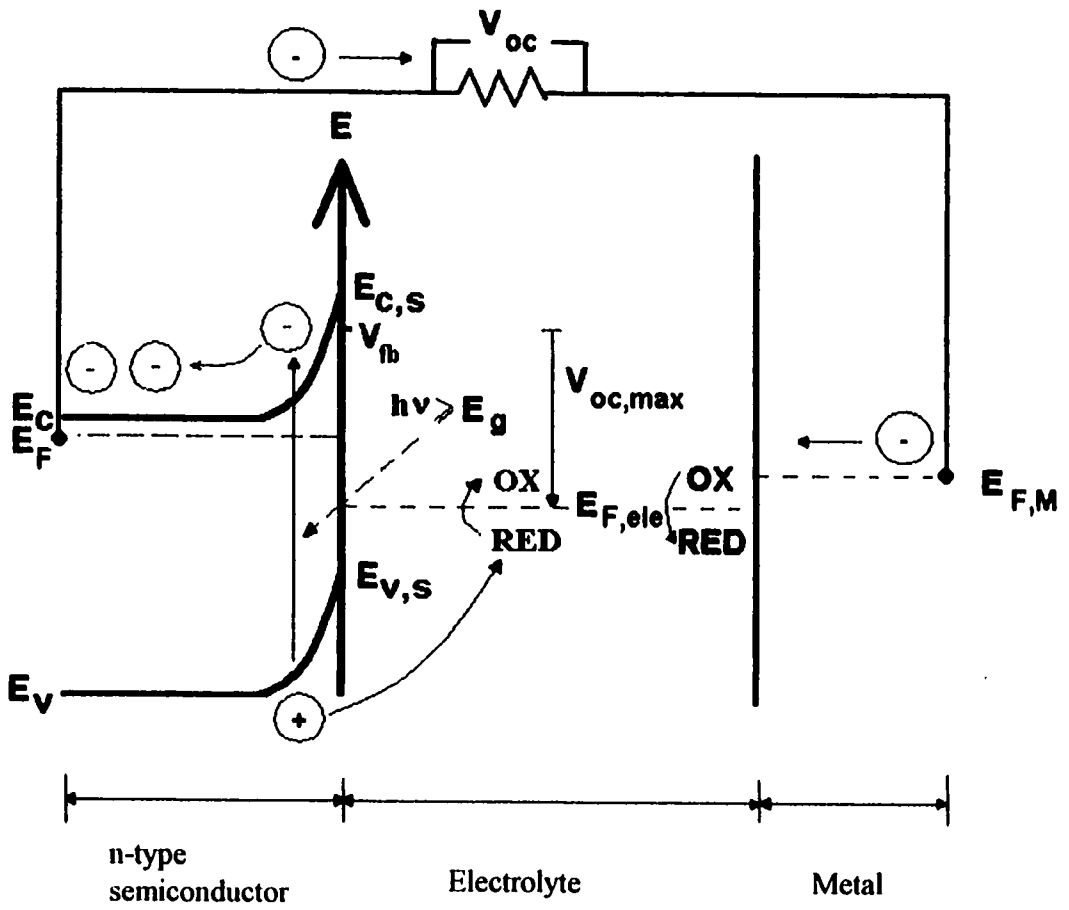

Fig. 1.8 Photocurrent generation at an n-type semiconductor. Photogenerated holes move to the surface and oxidize reduced species (RED) in the solution. Photogenerated electrons are directed toward the bulk of the semiconductor and reduced oxidized species (OX). V_{fb} = Flat band potential; $V_{oc,max}$ = maximum open-circuit photopotential; $E_{F,M}$ = Fermi level of the metallic counter electrode; $E_{v,s}$ = valence band energy at the surface of the semiconductor; $E_{c,s}$ = conduction band energy at the surface of the semiconductor.

$$RED + h^+ = OX \quad \text{(anode reaction)} \tag{1.12}$$

$$OX + e^- = RED \quad \text{(cathode reaction)} \tag{1.13}$$

No net chemical change is produced in the electrolyte, and electrical power is delivered to the external load through the photo-voltage and the photocurrent generated by the semiconductor electrode. The photo-generated current in the semiconductor consists of two basic components: (i) the current owing to carriers generated within the depletion region and (ii) the current arising from carriers generated in the bulk that diffuse into the depletion region.

If the incident photons are absorbed within the depletion layer, then the excited charge carriers are separated with minimum recombination and the photocurrent quantum efficiency (electrons collected per photon absorbed) approaches unity. The maximum open-circuit potential ($V_{oc,\ max}$) is given by the potential difference between the flat band potential and the potential corresponding to the electrolyte Fermi level (Figure 1.8).

The photocurrent versus applied voltage behaviour depends on the energy distribution of the incident photons, the absorption coefficient of the semiconductor, the diffusion length of the excited holes and electrons, and the recombination rate. As long as the depletion layer thickness exceeds the depth of charge carrier generation, then photocurrent quantum efficiencies are independent of the applied potential. As the applied potential approaches the flat band potential, V_{fb}, the depletion layer thickness decreases, increasing the level of electron-hole recombination and the probability of

electron transfer to the electrolyte oxidized species via the conduction band, enhancing dramatically the cathodic dark current.

1.8 Cadmium Chalcogenide Electrodes

One of the main classes of regenerative photoelectrochemical cells has been constructed by using cadmium chalcogenide photoanodes in aqueous solutions containing a chalcogenide/ polychalcogenide redox system, e.g., $CdX \mid X^{2-}/ X_n^{2-}$, where X = S, Se, Te and n is generally > 2. These materials have low band gap energies (1.4 eV < E_g < 2.4 eV: Table 1.2) and reasonable overlap with the solar spectrum. The cadmium chalcogenides' maximum theoretical conversion efficiencies under direct sunlight are shown in Figure 1.9.[41] The conversion efficiency of CdTe is greater than that of CdSe and much greater than that of the CdS.

Photoelectrochemical cells with solar energy power conversion (η) of up to 9.5 % (in aqueous 1M Cs_2S-S-NaOH) using single crystal materials have been reported.[42] However, due to the prohibitive cost of single crystal semiconductor materials, much effort has been devoted to develop stable PEC solar cells based on polycrystalline thin film semiconductor materials. n-CdSe has been used as a photo-anode in semiconductor liquid junction solar cells, both as a single crystal and in various polycrystalline forms.[42-48] The interest in CdSe comes from the fact that this material, when used in polycrystalline thin films, forms retains about 75% of the efficiency obtained in single crystals.[47] As we would like to use polycrystalline thin films for economic reasons and large area applications, CdSe is best suited for the purpose.

Table 1.2 Cadmium chalcogenide semiconductors band gap energy.

Semiconductor	Band gap energy, E_g (eV)	Wavelength, λ_g (nm)
CdS	2.4	520
CdSe	1.7	730
CdTe	1.4	890

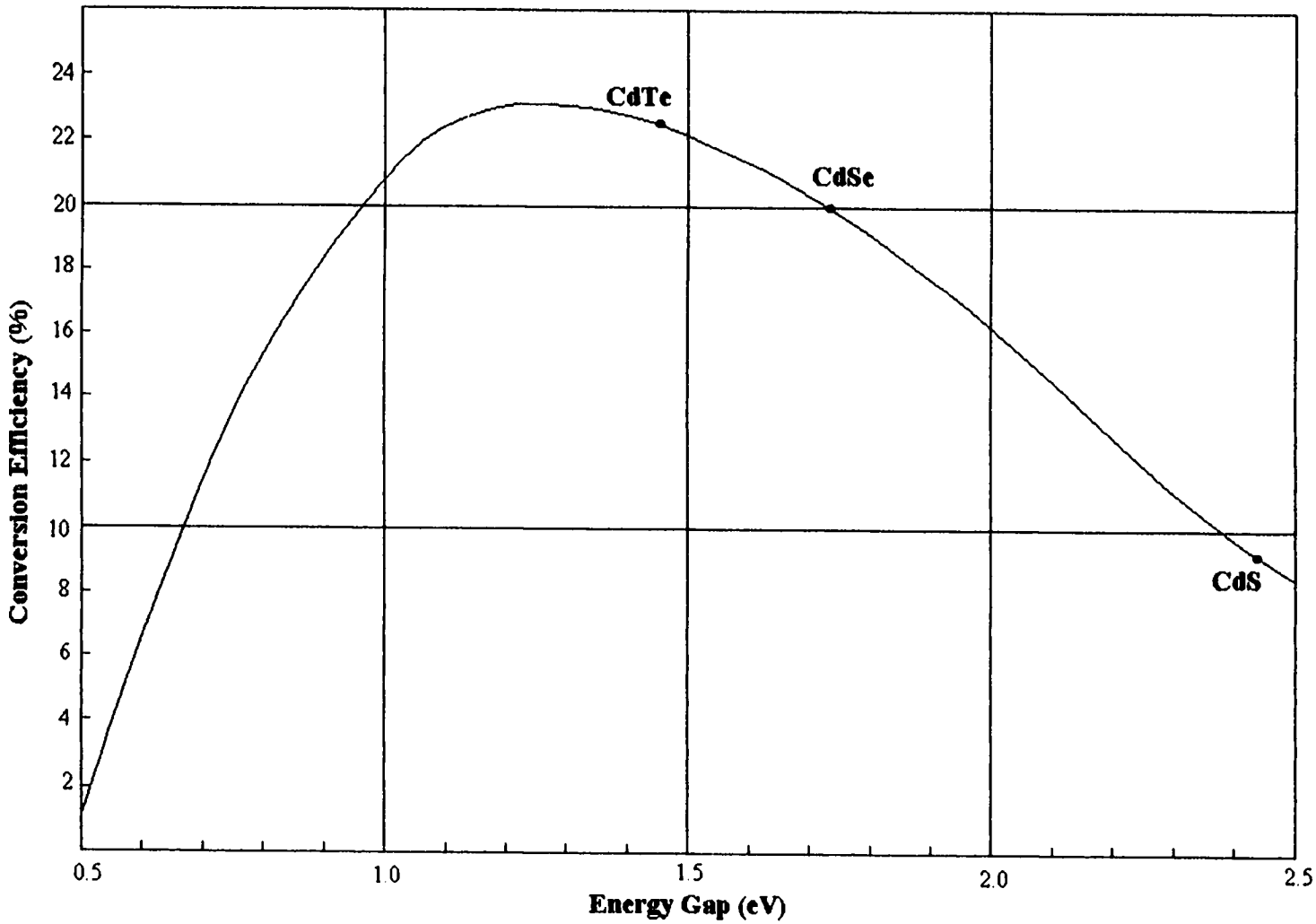

Fig 1.9 Maximum theoretical conversion efficiency of cadmium chalcogenides. [41]

Polycrystalline samples have been produced by such techniques as vacuum evaporation[49], electroplating[50], screen printing[91], chemical bath deposition[91], spray pyrolysis[91], and pressure sintering[51]. Based on the studies of Iwanov and Nanev,[52] concerning the direct synthesis of epitaxial II-VI semiconductor thin films on single crystal Cd and Zn substrates, another promising technique was developed. This method, referred to in the past as the "tarnishing reaction"[53] or as the "gas-solid process"[54], involves the reaction of the chalcogen vapour with the surface of a heated metal substrate, under constant argon flow. It has been demonstrated that the gas-solid process, in its early stage of development, enables the synthesis of polycrystalline films of CdS, CdSe, ZnS and ZnSe on a variety of substrates. The substrate can either be a plate of the metal itself (e.g., Cd) or be composed of the metal, deposited for example by evaporation, on a conductive gas plate (indium-tin oxide coated glass) or on another metal (titanium).

Through these preliminary studies, the metal substrates used in the synthesis of polycrystalline II-VI compounds were always maintained at temperatures below their melting points. For CdS and CdSe, the Cd substrates were kept at about 300^0C (melting point of Cd is 321^0C); for ZnS and ZnSe, the Zn substrates were kept at about 400^0C (melting point of Zn is 420^0C). At these temperatures, the reactions proceed as the chalcogen (X) vapours are brought in contact with the substrates' solid metal (M) surfaces under constant argon flow according to:

$$M_{(solid)} + X_{(vapour)} \xrightarrow{\Delta,\ Ar\ flow} MX_{(solid)} \qquad (1.14)$$

The thickness of the semiconductor layer obtained was shown to vary with the reaction time giving a maximum thickness of ~ 3 μm after 4 hours.[53,54,556] Of the group II-VI materials produced under these experimental conditions, CdSe gave the highest photovoltaic energy conversion efficiency, 1% (1M Na_2S / 1M S / 1M NaOH).[55]

In this thesis, we present the reaction of the metal substrate (Cd) with the chalcogen vapour (Se) that proceeds at a temperature a few degrees above the melting point of the metal substrate. For this reason, it is appropriate to call this method the liquid metal-vapour reaction (LMVR):

$$M_{(liquid)} + X_{(vapour)} \xrightarrow{\Delta,\ Ar\ flow} MX_{(solid)} \qquad (1.15)$$

This technique is promising because it has been shown to provide highly textured surface area layers that are assumed to be mainly responsible for the high energy conversion efficiency, 6.9% in 1M Na_2S/ 1M S/ 1M NaOH aqueous solutions.[19] In addition, it is a low temperature process and does not require high vacuum.

1.9 Electrolyte Used in this Work

Since 1976, several researchers [19,29,43-45,57] found that the aqueous polysulfide redox system (S_n^{2-}/S_{n+1}^{2-}: $nS_{n+1}^{2-} + 2e^- \rightarrow (n+1)S_n^{2-}$) can stabilize a number of low band gap n-type semiconducting photoanodes against photocorrosion, in particular CdS and CdSe. Previous work on sulfur-based cells has been limited to inorganic sulphur salts. Licht et al.[58-60] showed that CdSe in contact with an aqueous polysulfide electrolyte ($MOH/M_2S/S$) (M= Li, Na, K, or Cs) improves in efficiency and longetivity if Cs^+ is

used instead of Na^+ as the cation. It was shown experimentally that the dramatic variations in open-circuit voltage, short-circuit current and fill factor generally follow the trend Li (CdX/polysulfideS_x^{2-}) < Na < K < Cs.[92] The kinetics of polysulfide electrochemical redox reactions increase in parallel with the size of the accompanying cation according to the sequence $Li^+ < Na^+ < K^+ < Cs^+$. Cell efficiency and long term stability exhibit the same order. Recently, there has been considerably research interest in the thiolate/polysulfide redox couples. [33,61-65,68] For instance, they were studied as a novel type of cathode material in a solid polymer electrolyte lithium battery, [65] and could be potentially applied to all solid-state electrochemical photovoltaic cells.[33,68]

In this project, the redox couple used is the thiolate/disulfide system CsT/T_2 (Scheme 1),

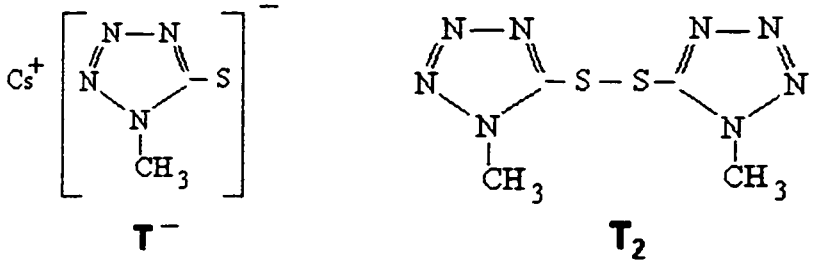

Scheme 1 Structure of the redox couple used in this work.

where CsT stands for 5-mercapto-1-methyltetrazole cesium salt and T_2 for its disulfide. Delocalisation of the negative charge on the sulfur and nitrogen atoms facilitates dissolution and dissociation of the alkali metal thiolate salt in aprotic media. The more positive potential of the CsT/T_2 redox couple (0.52 V vs. NHE in water or poly(ethylene glycol)[64]), in comparison to that of the inorganic polysulfides S_n^{2-}/S_{n+1}^{2-} (-0.34 V vs.

NHE in a PEO-based polymer electrolyte[66]), should give the cell an enhanced open-circuit photo-potential. Reactions in EPC using an n-CdSe semiconducting electrode may be written as follows:

(Photo-anode)

$$n\text{-}CdSe \xrightarrow{2h\nu} 2e^- + 2h^+ \qquad 1.16$$

$$2T^- + 2h^+ \longrightarrow T_2 \qquad 1.17$$

(Cathode)

$$T_2 + 2e^- \longrightarrow 2T^- \qquad 1.18$$

Marsan and Malservisi[67] reported that the conductivity of the solid polymer electrolyte modified PEO-MT/T_2 (molar ratio of MT to T_2 is 10 to 1) (M= Li, Na, and K) measured at the same temperature increases with the atomic weight of the alkali cation. Recently, it has been shown that the electrolyte containing the cesium cation is still more conducting.[68] This is the reason why Cs^+ was chosen to be the cation in this project.

T^-/T_2 redox couple dissolves very well in dimethyl sulfoxide (DMSO).[69] However, DMSO has a high viscosity (2.00 mPa·s), which causes the electrolyte to have a low ionic mobility and therefore a high resistance. To improve the conductivity of the gel electrolyte, dimethyl formamide (DMF), that has a much lower viscosity than that of DMSO (0.8 mPa·s), is introduced as a co-solvent. It should be remembered that a gel electrolyte can eliminate the photocorrosion process in an EPC because of its low solvation energy for the semiconductor lattice cations. Furthermore, as in the case of

solid polymer electrolytes, gel electrolytes allow the fabrication of very thin cells (compact devices), which leads to a lower absorption of visible light by the electrolyte.

It was found that as the concentration of CsT increases, the conductivity of the gel electrolyte increases, and as more T_2 is put into the electrolyte, the conductivity is decreased.[69] At high concentrations of T_2, e.g., CsT/T_2 molar ratio of 1, the conductivity is decreased very sharply, the electrolyte becomes more yellow and absorbs much more visible light, hence decreasing the cell energy conversion efficiency. On the other hand, a high enough concentration of T_2, e.g., CsT/T_2 molar ratio of 10/1, is needed to improve the reduction kinetics at the counter-electrode, and therefore the cell performance. Based on these results and analysis, the following composition for the liquid electrolyte incorporated in the polymer matrix (gel electrolyte) is used in order to balance above advantages and disadvantages regarding the concentration of T_2 and the properties of DMSO and DMF: DMSO/DMF/CsT:T_2 with weight ratio DMSO/DMF = 40/60, solvent to cesium salt molar ratio O/CsT = 10/1 (O represents the oxygen atom in DMSO and DMF), and molar ratio of CsT: T_2 = 10:1. At an O/CsT ratio of 10/1, the solution is saturated. At a CsT/T_2 ratio of 10:1, a little bit of conductivity will be sacrificed in order to have better reduction kinetics at the transparent counter-electrode.

The gel electrolyte is prepared by incorporating the above liquid electrolyte in a polymer matrix. In this project, poly (vinylidene fluoride) (PVDF), $(-CH_2-CF_2-)_n$, was chosen as the polymer because it offers the extraordinary combination of toughness and flexibility. PVDF-based gel electrolytes also show a good resistance to UV irradiation and are therefore well suited for commercial applications, e.g., photo-electrochemical

devices.[70] Optically transparent samples with reasonable mechanical properties can be prepared from a number of salted organic solvents, with most PVDF-based gels exhibiting conductivity of ~10^{-3} S·cm^{-1} at ambient temperature.[71] PVDF was introduced in the liquid electrolyte at a weight content of 20%. The mechanical and electrical properties of this electrolyte have been reported to be very interesting at room temperature.[72] Its ionic conductivity (σ) is governed by the conductivity of the liquid electrolyte incorporated in the polymer: $\sigma_{gel} = 0.66 \cdot \sigma_{liquid}$. The conductivity of this gel electrolyte is 7.3 x 10^{-3} S·cm^{-1} at 22^{0}C,[72] which is very interesting for the application discussed in this thesis.

1.10 Counter-Electrode Used in this Work

In this project, commercial indium-tin-oxide (ITO) conducting glass was used as a counter-electrode. The ITO electrode is composed of a thin oxide film (8 μm thick) coated on glass. It is transparent with a transmittance of 90% under white light illumination and highly conducting. The photovoltaic cell conversion efficiency can however be limited by the oxidized species (T_2) reduction kinetics at this electrode. Studies of the electrochemical properties (redox behaviour, kinetic reversibility) of the redox couple at the ITO electrode have been done in a previous work.[69] Cyclic voltammetry performed on a PVDF-based gel electrolyte is shown in Figure 1.10.[72] The fact that the anodic and cathodic peak separation, ΔE_p, is large (ΔE_p = 2.7 V >> 59/2 mV) and that increases with the sweep rate (not shown in Fig. 1.9) indicates that the

electrochemical reversibility of the T^-/T_2 redox couple at ITO is poor (slow electrode reaction) in the gel electrolyte. The high peak-to-peak separation implies that some chemical transformation is coupled with electron transfer and that the ohmic drop is significant in this medium. It is also found that the oxidation process is more difficult in the gel than in the liquid media (without PVDF) whereas the reduction process is easier in the gel.[69] Despite the above results, ITO is used in this work in order to compare the behaviour of similar EPCs based on LMVR and electrodeposited CdSe electrodes.

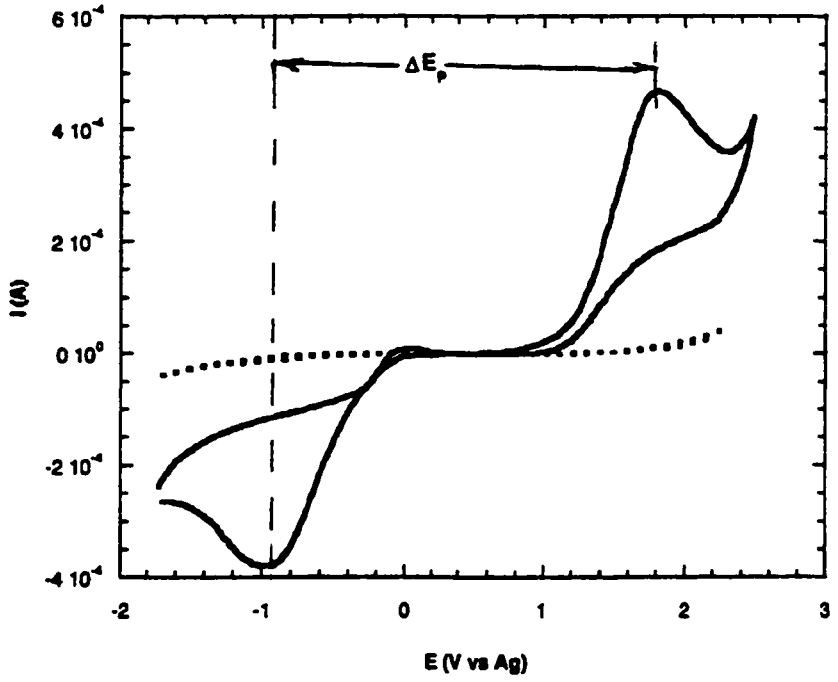

Fig. 1.10 Cyclic voltammogram of a gel electrolyte at the ITO electrode.[73]
Composition of the gel:
[PVDF(20%),(DMSO:DMF)(40:60)(80%)] containing 0.1M TBAP only (.....) and 0.1 M TBAP, 50 mM CsT, and 5 mM T_2 (___);
sweep rate: 100 $mV \cdot s^{-1}$.

1.11 Objectives of the Project

The main objective of this project is to develop an electrochemical photovoltaic cell which has a long life time, relatively high energy conversion efficiency, and low cost. During this project we have been engaged in a major effort to produce efficient polycrystalline n-CdSe photoanodes by liquid metal-vapour reaction. Once we were able to produce an efficient set of reproducible electrodes, we then characterized them using different analysis tools: chemical (crystalline structure and Cd:Se ratio: X-ray diffraction; semi-quantitative analysis: energy dispersive analysis of x-ray, EDAX), physical (morphology: scanning electron microscopy), optical (band gap energy: short-circuit photocurrent vs. hv) and electrochemical (type of semiconductivity: cyclic voltammetry). In view of their performance and reproductibility, we devoted time to compare their properties to that of n-CdSe photoanodes made by electrodeposition. The next step was to assembly the electrochemical photovoltaic cells in a glove box and to perform photoelectrochemical measurements in the dark and under illumination for the determination of: (i) the short circuit density (i_{sc}), (ii) the open-circuit potential (V_{oc}), (iii) the maximum power of the cell (P_{max}), (iv) the fill factor ($ff = P_{max}/(i_{sc} \cdot V_{oc})$), and (v) the energy conversion efficiency ($\eta = (V_{oc} \cdot i_{sc} \cdot ff)/P_{inc}$, where P_{inc} is the incident power). The results obtained previously with the cell n-CdSe (electrodeposited)/PVDF-based gel electrolyte/ITO[73], are shown in Figure 1.11. In the dark, the cell behaves as a diode with a much more significant cathodic current than anodic current, which is typical of a Schottky junction between an n-type semiconductor and a metal or an electrolyte. When illuminated with a white light (incident power: 30 $mW \cdot cm^{-2}$), the following results were

obtained: (i) i_{sc} = 1.1x10^{-2} mA·cm^{-2}; (ii) V_{oc} = 0.39 V; (iii) P_{max} = 5.0x10^{-4} mW·cm^{-2}; (iv) ff = 0.12; (v) η = 1.7x10^{-3} %.[73] These characteristics will be compared with those obtained with the cell, n-CdSe (LMVR) / PVDF-based gel electrolyte / ITO.

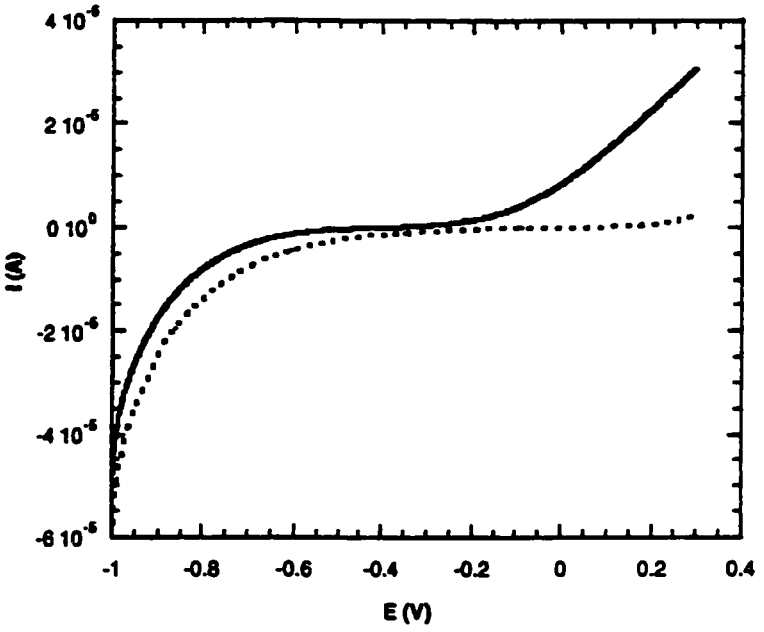

Fig. 1.11 Current-voltage curves of the PEC n-CdSe (electrodeposited)/gel electrolyte/ITO, obtained in dark (.....) and under illumination (___) at 22^{0}C.[73] Composition of the gel: [PVDF(20%),(DMSO:DMF)(40:60)(80%)] with O/CsT = 10/1 and 1.34 M CsT:0.13 M T_2 . CdSe surface area: 0.79 cm^2; power of incident light (tungsten halogen lamp): 30 mW.cm^{-2}; sweep rate: 1 mV·s^{-1}

CHAPTER 2

EXPERIMENTAL

2.1 Preparation of CdSe Semiconducting Electrodes

2.1.1 Cadmium Substrates

1 x 1 cm cadmium substrates were cut from a 1 mm thick plate of Cd (99.999%, JOHNSON MATTHEY). The substrates had been carefully cleaned with acetone and then etched for 1 minute in a 5:4:1 mixture of H_2O:HCl:HNO_3 to provide a slight surface roughness. After that, they were thoroughly rinsed with deionised water followed with methanol, and then quickly dried with nitrogen before being introduced in the reaction chamber.

2.1.2 Muffle Furnace and Reaction System

The liquid metal-vapour reaction system is illustrated in Figure 2.1:

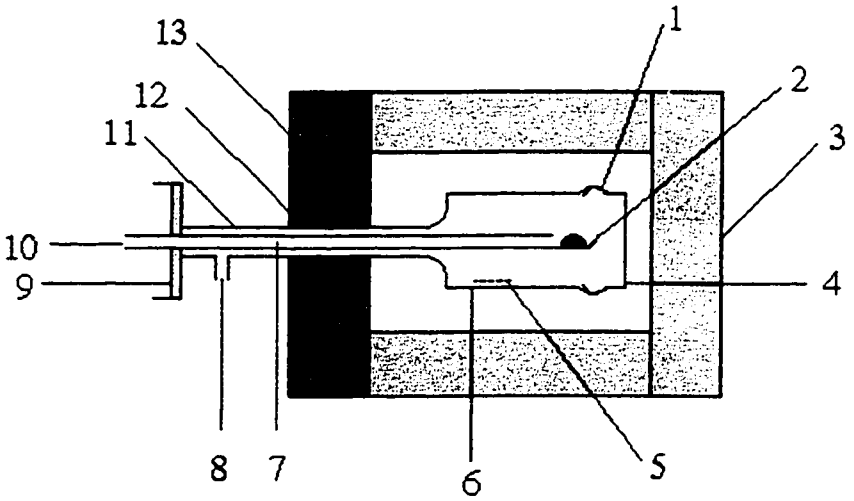

Figure 2.1 Liquid metal-vapor reaction system.

(1) Reaction chamber (quartz or Pyrex).

(2) Selenium source.

(3) Muffle furnace (specifically designed for these experiments, equipped with a programmable microprocessor temperature control, 1 zone).

(4) Thermocouple of muffle furnace.

(5) Cd substrate.

(6) Thermocouple (OMEGA HH-52).

(7) Inner tube (quartz or Pyrex, acts simultaneously as gas inlet and as the spoon containing selenium).

(8) Argon outlet.

(9) Torion sliding joint (enables the inner tube to be retracted from the reaction chamber to position the selenium source outside the muffle furnace, while the reaction chamber is kept inside the muffle furnace).

(10) Argon inlet.

(11) Reaction chamber outer tube, extending to the exterior of the muffle furnace through hole in the muffle furnace door.

(12) Hole in the centre of the muffle furnace door.

(13) Muffle furnace door (reaction chamber can be removed or introduced in the muffle furnace by pulling back or pushing forward the muffle furnace door which is guided by two parallel metal roads attached to the furnace).

2.1.3 Liquid Metal-Vapour Reaction

This technique involves the reaction of selenium vapours with the surface of a heated cadmium substrate under constant argon flow. The Cd substrate is kept at a temperature a few degrees above its melting point (mp: 321^{0}C) and the reaction proceeds as the selenium vapour is brought in contact with the liquid cadmium surface according to the following equation:

$$Cd_{(liquid)} + Se_{(vapor)} \longrightarrow CdSe_{(solid)} \qquad (2.1)$$

In order to remove O_2, the reaction chamber containing the Cd substrate is purged for 30 minutes at 80 $cm^3 \cdot min^{-1}$ with ultra-high purity Ar. Ar is introduced in an inner tube that acts simultaneously as the gas inlet and as the spoon containing the Se shot (Alfa Products 00290 Selenium Shot 1.6 mm). The reaction chamber is placed into the muffle furnace equipped with a programmable REXP-100 microprocessor temperature control. After purging, the Ar flow rate is reduced to 35 $cm^3 \cdot min^{-1}$. The Cd substrate is then heated to 325^{0}C over 30 minutes and the reaction proceeds for 4 hours (optimal conditions) as the Se vapour is brought in contact with the Cd surface. The CdSe sample is then allowed to regain room temperature under an Ar atmosphere.

2.1.4 Ohmic Contact

In order to ensure a good ohmic contact with the electrodes, a copper ribbon was attached with silver paint to the back of the semiconductor CdSe samples. The electrodes

were then glued to a 2.5 x 1.5 cm microscope glass slide with epoxy patch, leaving about 1 cm^2 of the CdSe exposed for the analyses.

2.2 Preparation of ITO Electrodes

Indium-tin-oxide (ITO) electrodes were cut from a piece of glass on which is deposited (only on one side) a thin film of indium-tin oxide (ITO, 7-14 Ω/□, Libbey Owens Ford). The size of the ITO electrodes was 2.5 x 1.5 cm (thickness = 2 mm). The ITO surfaces were connected to a copper ribbon using silver paint. The electrodes were then cleaned with soap and water, and rinsed with water and acetone. The last step was to immerse the electrodes in dichloromethane (CH_2Cl_2, BDH) in an ultrasonic bath (Cole-Parmer, model 8846-40) for 2 minutes. The electrodes were then dried in air.

2.3 Characterization of CdSe Electrodes

2.3.1 Surface Morphology

A HITACHI (S-2300) scanning electron microscope was used to observe the surface structure of the CdSe thin films. Micrographs were taken using a KEVEX X-ray analyzer with imaging capability.

2.3.2 Composition of CdSe Films

Semi-quantitative chemical analyses of CdSe thin films were carried out using the energy dispersive analysis of X-rays techniques (EDAX). For this analysis, a X-ray

detector located in the electron microscope (Hitachi S-2300) was used. Detection of these X-rays permits the identification of elements present in the sample and their concentration. Since the film is not destroyed by EDAX, it could be analysed afterward by X-ray diffraction (XRD).

2.3.3 X-Ray Diffraction

The crystalline structure of CdSe thin films was determined by X-ray diffraction using a MODEL D5000 SIEMENS diffractometer using radiations $K_{\alpha 1 \alpha 2}$ ($K_{\alpha 1}$: λ = 1.789Å) emitted by a cobalt source. The diffraction patterns were obtained at a speed of $2\theta = 0.5^0$ / min for Bragg angle values of $5^0 \leq 2\theta \leq 100^0$. DIFFRAC AT, software that permits elimination of the presence of ray diffraction due to $K_{\alpha 2}$ radiation, was used to visualise the diffraction patterns.

2.4 Synthesis and Characterization of the Redox Couple (CsT and T_2)

2.4.1 Synthesis of CsT

The protocol used for the synthesis of the 5-mercapto-1-methyl tetrazole cesium salt (CsT) was developed in Dr. Marsan's laboratory at UQAM. The cesium salt used in this project is prepared via the following reaction:

$$2HT_{(aq)} + Cs_2CO_{3(aq)} \longrightarrow 2CsT_{(aq)} + H_2O_{(l)} + CO_{2\,(g)} \qquad (2.2)$$

$3x10^{-3}$ moles of cesium carbonate (Cs_2CO_3) (Aldrich, 99.99%) were dissolved in nanopure water and gradually added to a solution containing $6x10^{-3}$ moles of 5-mercapto-

1methyl-tetrazole (HT) (Aldrich, 98%) with stirring. The solution containing CsT was evaporated using a rotary evaporator (Buchi R110). The solid was dissolved in acetonitrile (Fischer Scientific, H.P.L.C. Grade) to filter out the unreacted reactants. The solution was then evaporated to give the white product, CsT, which was dried in the oven at 100^0C for 12 hours, placed in a dessicator under vacuum with P_2O_5 (Biopharm A.C.S.) for another 12 hours, and then put in a glove box.

2.4.2 Synthesis of T_2

The synthesis of the disulfide T_2 is based on the following reactions:

$$HT_{(aq)} + NaOH_{(aq)} \longrightarrow NaT_{(aq)} + H_2O_{(l)} \quad (2.3)$$

$$2NaT_{(aq)} + I_{2(aq)} \longrightarrow T_{2(s)} + 2NaI_{(aq)} \quad (2.4)$$

1 mole of HT (Aldrich,98%) was deprotonated by adding 1 mole of NaOH (Aldrich, 98%) aqueous solution. The reaction took place for 30 minutes while it was stirred. $7.5x10^{-2}$ moles of 5-mercapto-1-methyltetrazole sodium salt (NaT) (Aldrich, 97 %) were dissolved in hot nanopure water (50^0C). $3.0x10^{-2}$moles of solid I_2 (Aldrich, 99.8 %) were added gradually to the stirred NaT aqueous solution until the reaction is complete. When the solution was cooled down, the white product, T_2, crystallized. The precipitate was washed with nanopure water and then with ethanol (Alcool de commerce). The product was dried in the oven at 50-70^0C for 12 hours, placed in a dessicator under vacuum with P_2O_5 for another 12 hours, and put in a glove box.

2.4.3 Characterization of CsT and T_2

The purity of the two compounds was determined using infrared spectroscopy (FTIR, BOMEM, Hartmann & Braun, MB-SERIES) between 4000 and 400 cm^{-1} and melting point measurements (Fisher Johns, 12-144V2, 4005). FTIR spectra and melting points (CsT: 196^{0}C; T_2: 111^{0}C) were very close to those obtained previously in our laboratory.

2.5 Preparation of the Liquid and Gel Electrolytes

All the solutions were prepared in ambient atmosphere with the exception of the gel electrolyte. The latter was prepared in a glove box under nitrogen atmosphere.

2.5.1 Preparation of the Liquid Electrolytes

The preparation of the liquid electrolytes demands particular experimental conditions such as a non-aqueous medium. The solvents that we used were kept on drying agents (dimethylsulfoxyde, DMSO, Anachemia Accusolv, 99.9%) or under nitrogen in a bottle with a septum (anhydrous dimethylformamide, DMF, Aldrich, 99.8 %). In this work, the CsT concentration is expressed in terms of an O/Cs (solvent/Cs) molar ratio of 10/1, calculated using the formula (2.5)[74]:

$$\frac{O}{Cs} = \frac{\text{mass of solvent (g)}}{\text{molecular weight of the solvent (g/mol)}} \times \frac{\text{molecular weight of CsT (g/mol)}}{\text{mass of CsT (g)}} \times n \qquad (2.5)$$

where n represents the number of atoms of oxygen in DMSO and DMF susceptible of interacting with the alkali cation (n = 1 for both solvents). This salt concentration corresponds to 1.34 M. The CsT/T_2 molar ratio is kept at a value of 10/1, therefore the concentration of T_2 is 0.13 M. For some experiments, HT was used instead of CsT at the same concentration (1.34 M). The appropriate quantities of CsT (or HT) and T_2 were dissolved in DMSO/DMF (40%/60% v/v) solvent mixture and stirred. The two compounds were first dissolved in DMSO, and then DMF was added to the solution. The anti-chamber of the glove box is always flushed to remove oxygen before the introduction of chemicals. This removes possible traces of atmospheric oxygen from the liquid electrolyte.

2.5.2 Preparation of the Gel Electrolytes

The presence of an inert atmosphere must be maintained during the preparation of the gel electrolytes because all the chemicals are sensitive to water and oxygen. More than that, if the solution is in contact with air, there is a progressive evaporation of the solvents and therefore an increase in the viscosity of the solution. As a consequence, the ionic conductivity decreases rapidly.[75] Under these circumstances, all the manipulations were done in a glove box (Plas Labs model 818GB 220, Fisher Scientific) under an ultra-dry nitrogen atmosphere. Poly (vinylidene fluoride), PVDF (Aldrich, molecular weight ≈ 534000 g/mol), was dried at 50^0C for 24 hours[76], and then introduced in the glove box. Once the liquid electrolyte was prepared, PVDF was gradually added to the solution with

stirring. To obtain a homogeneous composition, the solution was heated up to 60^0C on a hot plate (viscous solution) and then cooled down at room temperature to form the gel.

During preparation of the gel electrolytes, two parameters must be kept under control: the temperature and the quantity of polymer that we add. The temperature has an important effect on the transparency of the gel electrolytes: when temperature is raised above 60^0C, the gels become semi-transparent on cooling and when the temperature reaches 75^0-80^0C, the gels become hard and opaque (brown). The polymer was introduced in the liquid electrolytes at a weight content of 20%, calculated as follows:

$$\mathbf{m}_{PVdF} / (\mathbf{m}_{PVdF} + \mathbf{m}_{DMF+DMSO}) = 0.20 \qquad (2.6)$$

where **m** represents the mass in grams. The percentage of polymer is also an important factor because over 20%, incorporation of PVDF in the liquid electrolytes becomes very difficult and the gels have the appearance of hardened pastes. Moreover, if we increase the quantity of polymer too much the ionic conductivity decreases. On the other hand, lower polymer content makes the gels too liquid. In conclusion, the gel composition is the result of a judicious compromise in order to obtain an electrolyte with both good mechanical properties and high conductivity.

2.6 Fabrication of the Cell

Once a CdSe electrode has been prepared, its introduction into a photoelectrochemical cell involves physical arrangement of the electrode, attachment of the electrical leads and encapsulation for environmental protection. If

photoelectrochemical cells are to be practical for terrestrial applications, they must be done on a mass production basis at reasonable cost. For example, much of the recent effort in the development of fuel cell technology has been devoted to reducing the thickness of cell components while refining and improving the electrode structure and the electrolyte phase, with the aim of obtaining a higher and more stable electrochemical performance while lowering cost.

The cell fabrication process described here has been realized in a glove box for the reasons explained in section 2.5. Typically, a cell is constructed as shown in Figure 2.2 and has the final appearance seen in Figure 2.3. After attachment of a copper ribbon to the CdSe electrode, the latter is glued on a 2.5 x 1.5 cm microscope glass slide with epoxy patch glue. The counter electrode is indium-tin-oxide coated glass having a resistance of about 7-15 Ω / $\square$ (Libley Ouens Ford); a copper wire is used to form an electrical contact. A layer of parafilm (thickness = 0.14 mm) with a hole (A= 0.2 cm^2) is put on this surface. The hole permits the contact between CdSe electrode, gel electrolyte and counter electrode, and also provides the illumination area. 0.06 ml of gel electrolyte were deposited on the surface of the CdSe electrode with a syringe. The counter electrode was then pressed against the exposed surface of the gel while it was warm, in such a manner as to avoid entrapment of air bubbles. This could be observed through the transparent electrode during its application. To complete the device fabrication, the whole cell was sealed with epoxy glue.

Such a cell poses many challenges involving both device design and fabrication. The challenge in the device design is to make a cell that is thin and thus much cheaper, especially for mass production. The challenges in the cell fabrication are to establish

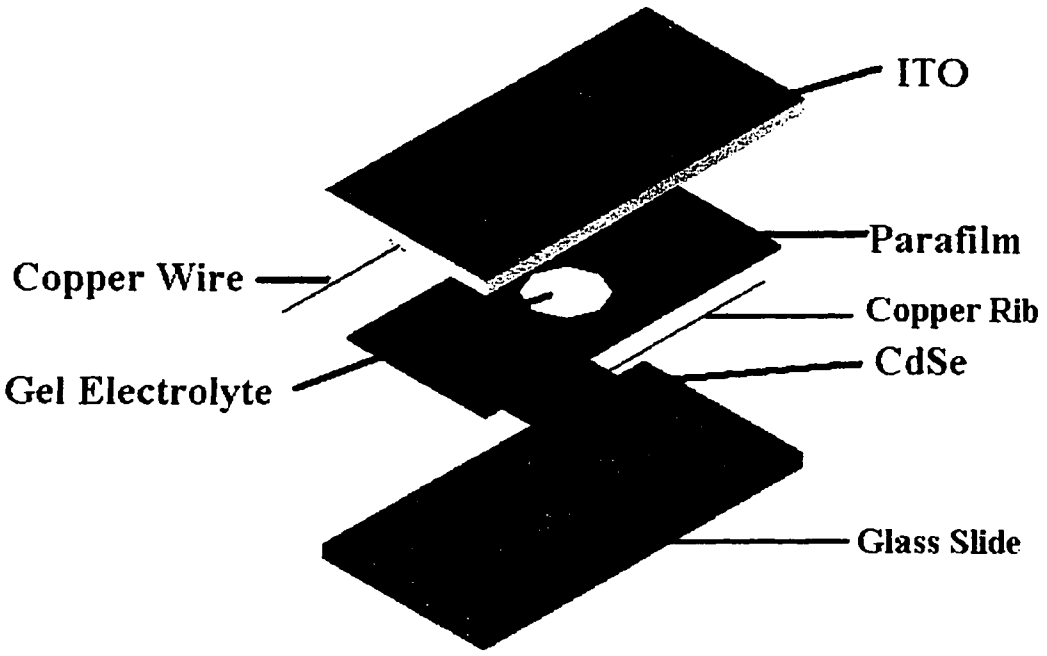

Fig. 2.2 The exploded form of a photoelectrochemical cell.

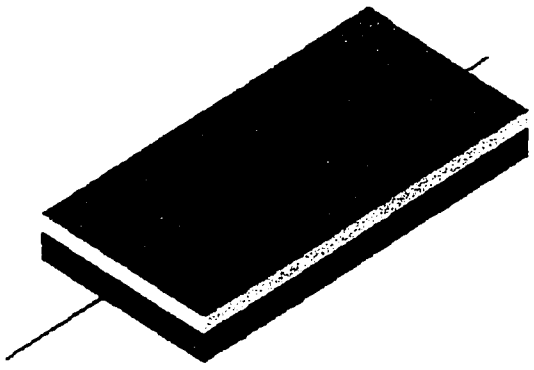

Figure 2.3 Compact cell.

good electrical contacts, that the excess of gel will not produce a short circuit at the contact with the metallic cadmium support and that the sealing operation of the cell is done properly

A short circuit can be prevented by carefully covering the backside of the semiconductor with epoxy patch glue. In addition, the choice of the glue is another important factor. Epoxy patch glue limits solvent evaporation and prevents the excessive drying of gel over long periods of time. The key in obtaining an operational cell is also to cause the least damage to the surface of the CdSe electrode during the sealing process. Experiments have shown that such a cell design provides good electrical properties with mechanical strength and a minimum weight. In fabricating the cell, various alternatives are possible. In this project, we present what we consider to be the optimized steps followed in the construction of the cell.

Afterward, some effort has been done to design a cell that does not require the patch epoxy glue for sealing purposes. As shown in Figure 2.4, the cell design includes a "body" made from plastic that supports the internal cell components; the semiconducting electrode, CdSe, is placed at the bottom. An O ring, placed between this electrode and the ITO counter electrode, serves to seal the gel electrolyte within the device. The counter electrode was positioned in the space limited by the lateral wall of the plastic "body" and pressed against the surface of the gel layer with two screws. This process enables the O ring to completely adhere to the surface of the CdSe electrode and entrap the gel electrolyte between the two electrodes without leakage. Copper wires are connected to both electrodes to achieve electric contact. Processing time to fabricate the cell is reduced as compared to the prior cell design, but there is an increase in the size and weight of the

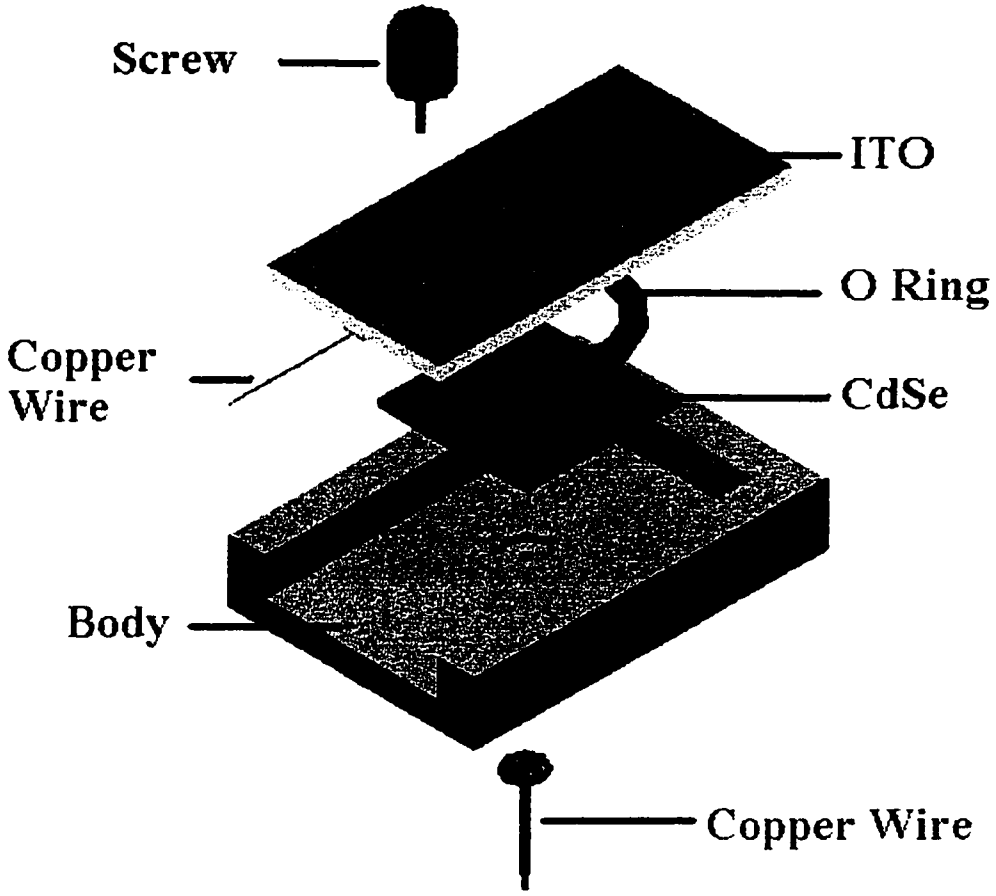

Fig. 2.4 New design of the cell

cell. The new design also presents the advantage of ease in taking apart all the components and replacing the CdSe electrode after long-term illumination. But the experimental work that was done using these devices shows that they are not as stable as desired. What could cause deterioration in cell performance is the air - gel electrolyte contact; therefore, it seems that there is no perfect sealing without glue. Although this design shows interesting possibilities, we no longer continued using it. Therefore, all our reported results will come from measurements made using the first typical cell (Figure 2.2).

2.7 Photoelectrochemical Measurement System

2.7.1 Cyclic Voltammetry in the Dark

Cyclic voltammograms, performed in the dark on n-CdSe /PVDF-based gel electrolyte /ITO cells, were obtained using the VoltaMaster 4 Electrochemical software version 3.04 (Radiometer Analytical S.A.). The experimental parameters were a potential range from –1.5 V to 1.5 V and a potential sweep of 1 mV/s or 10 mV/s for 3 to 10 cycles. These studies allowed the evaluation of the quality of the semiconductor/gel electrolyte junction (diode behaviour). This permits the determination of some key parameters of the cell such as the shunt resistance (R_{sh}), the rectification ratio (R_{rect}) and the diode ideality factor (n).

2.7.2 Cyclic Voltammetry under White Light Illumination

Cell performance was evaluated by measuring the open-circuit voltage (V_{oc}) and the short-circuit current density (i_{sc}), under white light illumination through the

semiconductor side using a 250 W halogen lamp. The system is shown in Figure 2.5. The illuminated area is 0.2 cm^2. The current-voltage characterization of the cell was carried out using VoltaMaster 4 Electrochemical software version 3.04. Neutral density filters were used to vary the intensity of the incident light. Light intensities were measured with an Optikon 88XLC photometer. Infrared radiation was filtered out by passing the light through a 12 cm water filter placed between the light source and the focusing lens. The plot of photocurrent vs. potential was used to determine the short-circuit current density (i_{sc}) when V=0, the open circuit potential (V_{oc}) when I=0, and the maximum power (P_{max}) when I ·V is maximal. The fill factor (ff) and the cell energy conversion efficiency (η) can be calculated using the following equations:

$$ff = \frac{P_{max}}{i_{sc} \cdot V_{oc}} \tag{2.7}$$

$$\eta\ (\%) = \frac{P_{max}}{P_{inc}} \times 100 = \frac{i_{sc} V_{oc} ff}{P_{inc}} \times 100 \tag{2.8}$$

where P_{inc} is the incident light power. All the measurements were performed at room temperature.

2.7.3 Spectral Response of the Cell

Monochromatic excitation was obtained using a 250 W halogen lamp and a Bausch & Lomb monochromator with a 10 nm band pass. The spectral response was obtained in the wavelength range 400-800 nm with the aim of determining the band gap

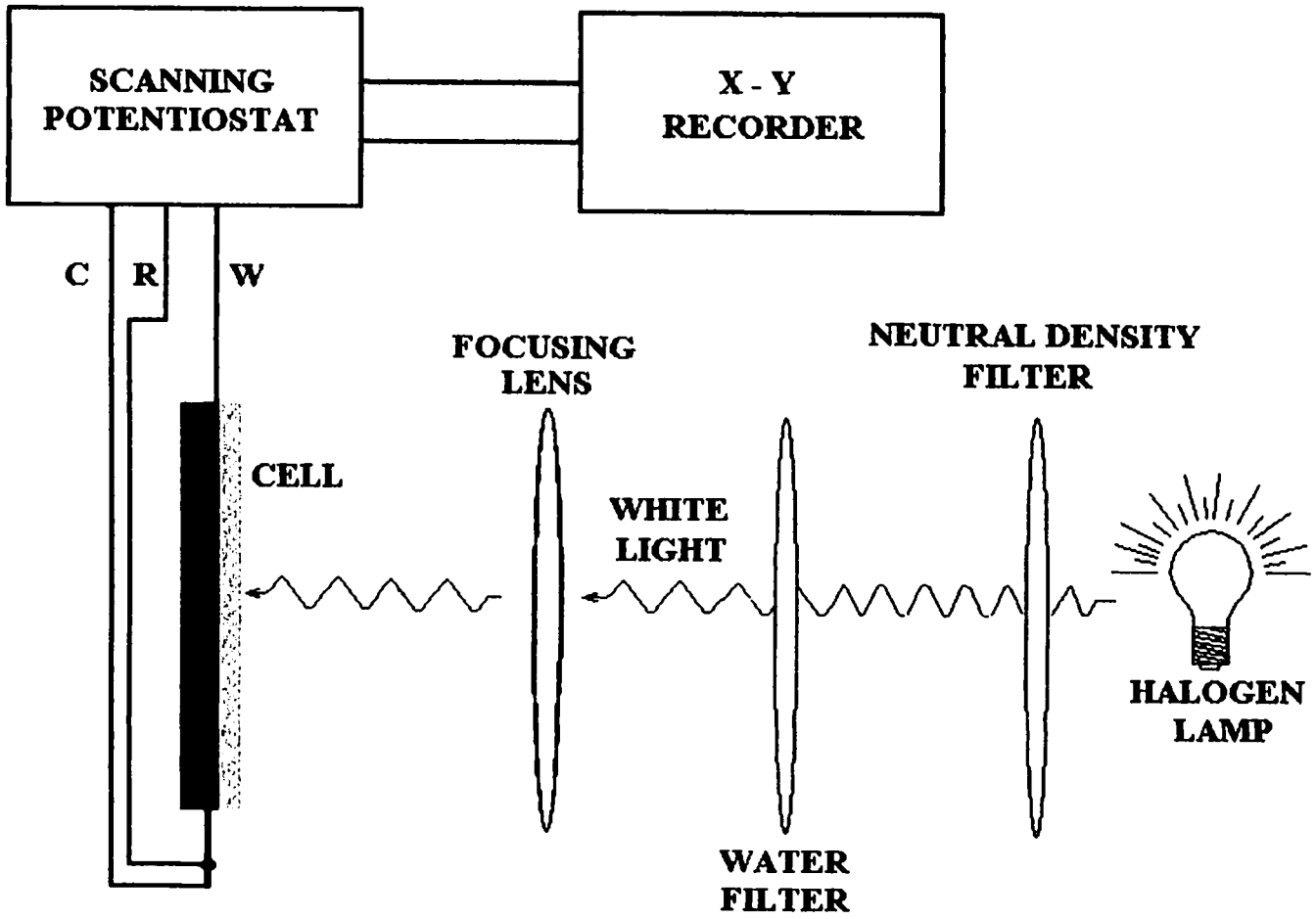

Fig. 2.5 **Photoelectrochemical measurement system. W = Working electrode; C = Counter electrode; R = Reference electrode.**

energy. Photocurrent measurements were monitored by a Keithley 617 programmable electrometer while changing the wavelength. No biasing was applied to the semiconductor electrode and no corrections were made for absorption and reflection losses

CHAPTER 3

STRUCTURAL, PHYSICAL AND CHEMICAL CHARACTERIZATIONS OF THE ELECTRODES

Energy conversion efficiency is very sensitively influenced by the crystallographic and morphological characteristics of the semiconductor(s) used. This chapter presents and discusses results of the structural (x-ray diffraction), morphological (scanning electron microscopy) and semi-quantitative analyses (EDAX) of CdSe thin films prepared by the LMVR method. The semiconducting properties are compared with those of CdSe layers obtained by electrodeposition.

3.1 X-ray Diffraction Patterns

Analysis of the diffraction patterns of a sample reveals the existence of different crystallographic phases in the film, their relative abundance, any preferred orientation and the lattice parameters. The identification of a species' crystalline structure from its x-ray diffraction patterns is based upon the position of the lines (2θ) and their relative normalized, integrated intensities. The diffraction angle 2θ is determined by the spacing between a particular set of planes, using the Bragg law:

$$2\,d \sin\theta = n\lambda \qquad (3.1)$$

where n is the order of the diffraction line and is numerically equal to the path difference for successive planes, λ is the wavelength, d is the interplanar spacing of the diffracting planes, and θ the Bragg angle. θ is the angle between the incident x-ray and the diffracting planes.

Literature illustrates that CdSe exists in hexagonal (wurtzite) and cubic (sphalerite) structures. CdSe films prepared by liquid metal-vapour reaction ($T = 330^0C$) may exhibit a mixture of hexagonal and cubic structures. The x-ray diffraction patterns (Figure 3.1) suggest a hexagonal phase growth with a preferential orientation of the (110): $2\theta_{obs} = 49.15^0$ and (112): $2\theta_{obs} = 58.39^0$ planes. The preferential orientation is determined from comparison of the values of the relative intensities of the peaks obtained in the diffraction pattern and the intensity values reported by Joint Committee on Powder Diffraction Standards (JCPDS) for hexagonal (wurtzite) and cubic (sphalerite) CdSe. High relative intensities of certain observed peaks is caused by the preferential orientation in the crystal. The diffraction pattern also reveals that the cubic phase may exist since its two major peaks overlap the most important peaks of the hexagonal structure. The cubic structure might be present with a preferential orientation of the (220): $2\theta_{obs} = 49.15^0$ and (311): $2\theta_{obs} = 58.39^0$ planes.

The x-ray diffraction studies performed on CdSe samples indicate that the position of the observed diffraction peaks corresponds reasonably well to those reported by JCPDS file for CdSe crystallizing in the hexagonal structure (Table 3.1). Their normalized integrated intensities, however, show little correlation when compared to those obtained with standard powder samples of hexagonal CdSe. The peaks are not that

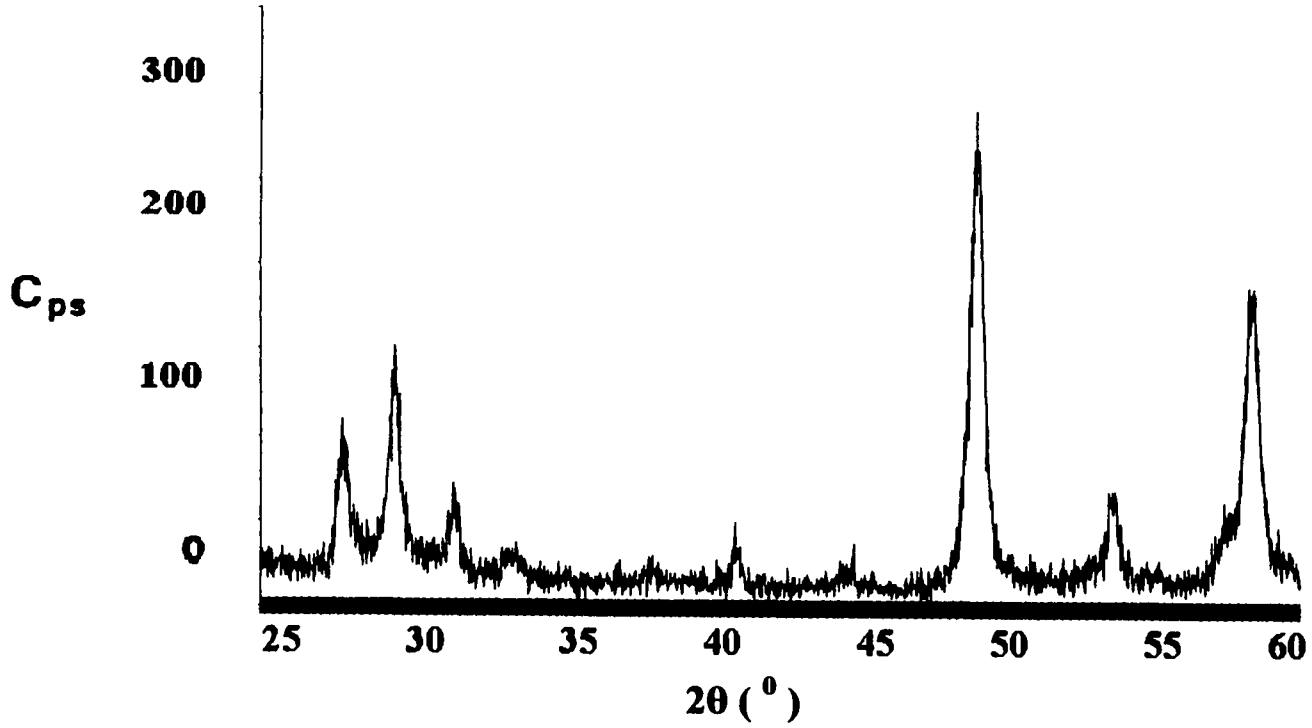

Fig. 3.1 XRD pattern of a typical CdSe electrode prepared by LMVR.

Table 3.1 Experimental X-ray diffraction peak positions , plane spacings , and relative intensities of CdSe sample made by LMVR compared to JCPDS values for hexagonal (wurtzite) and cubic (sphalerite) CdSe.

2θ Observed (^{O})	Calculated d-spacing (Å)	Relative Intensity (%)	Standard d-spacing (hkl plane) (Å)					
			CdSe [H][a]	I (%) [H]	CdSe [C][b]	I(%) [C]	Se [H][c]	Cd [H][d]
27.79	3.72	27.4	3.72 (100)	100				
29.53	3.51	41.3	3.51 (002)	70	3.51 (111)	100		
31.55	3.29	15.0	3.29 (101)	75				
33.60	3.00						3.00 (101)	
41.03	2.56	8.8	2.55 (102)	35				
44.76	2.34							2.34 (101)
49.15	2.15	100.0	2.15 (110)	85	2.15 (220)	55		
53.70	1.98	19.0	1.98 (103)	70				
58.39	1.83	64.4	1.83 (112)	50	1.83 (311)	25		

a Hexagonal structure[79]

b Face –centered cubic structure[78]

c Hexagonal structure[93]

d Hexagonal structure[94]

sharp and intense and this may indicate that CdSe electrodes are not so highly crystalline. It should be noted that small peaks appearing in the diffraction pattern of the CdSe samples were identified as corresponding to Cd and Se after they were compared with standard patterns. The presence of Cd ($2\theta_{obs} = 44.76^0$) can be associated with the fact that Cd substrate ($1cm^2$;1 mm thick) cannot react completely with selenium. The presence of Se ($2\theta_{obs} = 33.60^0$) is assumed to be introduced at the end of the vapour-liquid metal reaction during the process of cooling down the CdSe film. Se that didn't react might be seen on the surface of the Cd substrate. The hexagonal lattice parameters a and c were calculated from the observed d-spacing for the planes (110) and (112) by using: [77]

$$\frac{1}{d^2} = \frac{4}{3}\frac{(h^2 + hk + k^2)}{a^2} + \frac{l^2}{c^2} \qquad (3.2)$$

where h, k and l represent the Miller indices. The following values were obtained: a = b = 4.3 Å; c = 6.98 Å; c/a = 1.63. The parameter values are in fairly good agreement with the reference values: a = b = 4.3 Å; c = 7.02 Å; c/a = 1.63 reported in the literature[79] and they are also close to those reported for electrodeposited CdSe: a = b = 4.28 Å; c = 6.99 Å; c/a = 1.63.[68]

Figure 3.2 shows an x-ray diffraction pattern of polycrystalline CdSe made by electrodeposition, annealed in air at 550°C for 30 min and etched in 9M HCl for 20 seconds.[73] Comparison of Figure 3.1 and 3.2 indicates that CdSe electrodes made by electrodeposition show a different crystallinity and preferential orientation than CdSe electrodes made by liquid metal-vapour reaction. Table 3.2 gives the position (2θ, d-spacings of the diffraction planes), relative intensities and identification of the peaks. It also indicates that all the peaks of hexagonal CdSe are observed, with preferential

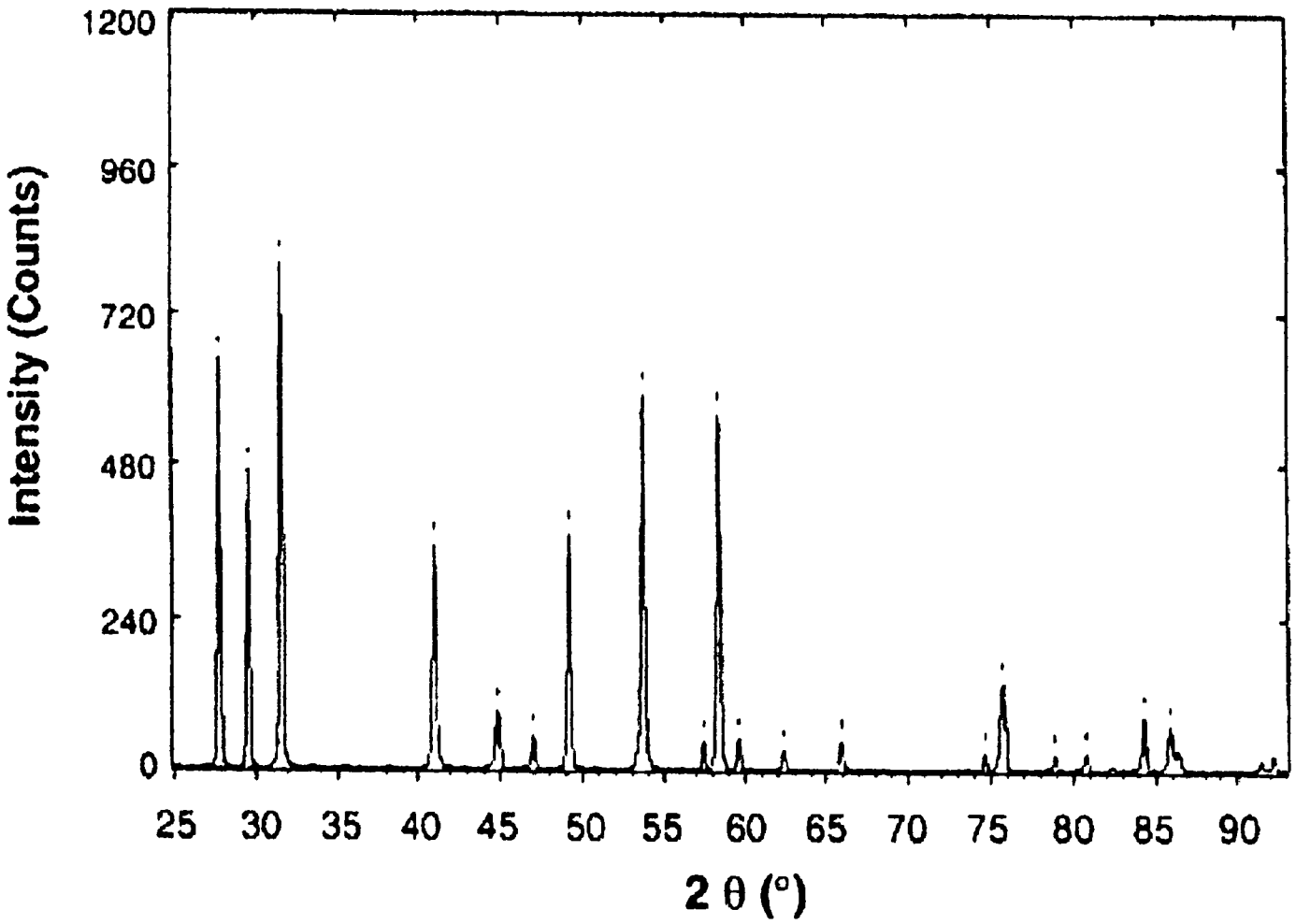

Fig. 3.2 XRD pattern of a typical CdSe electrode prepared by electrodeposition on titanium, annealed in air at 550^{0}C for 30 min and etched in 9M HCl for 20 s. [73]

Table 3.2 Identification of the X-ray diffraction peaks of the as-electrodeposited CdSe thin film. Substrate Ti; Conditions: annealed in air at 550^{0}C and etched in 9 M HCl[73].

2θ Observed (^{O})	Calculated d-spacing (Å)	Relative Intensity (%)	Standard d-spacing (hkl plane) (Å)			
			CdSe [H][a]	CdSe[C][b]	Cd [H]	Ti [H][c]
27.82	3.72	81	3.72 (100)			
29.58	3.50	59	3.51 (002)	3.51 (111)		
31.56	3.29	100	3.29 (101)			
41.01	2.55	44	2.55 (102)			2.56 (010)
44.84	2.34	12			2.35 (101)	2.34 (002)
47.01	2.24	7				2.24 (011)
49.18	2.14	47	2.15 (110)	2.15 (220)		
53.71	1.98	74	1.98 (103)			
57.43	1.86	6	1.86 (200)			
58.38	1.83	70	1.83 (112)	1.83 (311)		
59.59	1.80	6	1.80 (201)			
62.36	1.72	4				1.73 (012)
65.92	1.64	6	1.64 (202)			
74.66	1.47	3				1.48 (110)
75.74	1.46	18	1.46 (203)			
78.90	1.41	3	1.40 (210)			
80.81	1.38	4	1.38 (211)			
84.32	1.33	11				1.33 (103)
85.91	1.31	9	1.31 (105)		1.32 (112)	

[a] Hexagonal structure[79] . [b] Face-centered cubic structure[78] . [c] Hexagonal structure[80]

orientation of the (101), (102), (103) and (112) planes. The diffraction pattern of CdSe made by electrodeposition also indicates that the cubic structure might be present with a preferential orientation of the (311) plane. The diffraction lines which are not attributed to CdSe are assigned to metallic cadmium and to the titanium support (hexagonal phase).[95]

An easy way to establish that the CdSe samples obtained by electrodeposition are more crystalline than the CdSe samples obtained by LMVR is to compare the intensities and the shape (width) of the peaks. The diffraction patterns presented in Figure 3.1 and Figure 3.2 show more intense peaks for the CdSe sample prepared by electrodeposition. The peak width in an x-ray diffraction pattern is related to the size of the crystallites that compose the material via the Scherrer's formula[77] :

$$S = \frac{0.9\,\lambda}{B\cos\theta} \tag{3.3}$$

where S is the average crystallite size, λ is the wavelength of the radiation source and B is the full width at half maximum (FWHM) of a given diffraction peak, it can be noticed that the electrodeposition method yields larger crystallite sizes for CdSe electrodes (sharp peaks of high intensity) and hence reduces the number of grain boundaries within the polycrystal. The FWHM is the angular distance between the two points on the two slopes halfway between the base and the top of the peak. When analyzing a peak from the diffraction patterns obtained for CdSe made by electrodeposition (the peak in the proximity of $2\theta^0 = 58.38^0$), the value calculated for FWHM is 0.37^0. The corresponding peak from the diffraction pattern obtained for CdSe made by LMVR gives a value of

0.62^0 for the FWHM. Given that the FWHM of this peak is almost twice the size of the FWHM of the peak from the diffraction pattern of CdSe made by electrodeposition, and also that the peak is less intense we can conclude that the CdSe electrodes prepared by electrodeposition present a better crystalinity and therefore a much lower number of grain boundaries within the polycrystal. Hence the recombination of e^--h^+ pairs is most likely to be expected in the case of CdSe photoanodes prepared by LMVR.

3.2 Scanning Electron Micrographs

Comparative morphological studies on CdSe made by LMVR and ED were done. Figure 3.3 illustrates the surface morphology of a typical CdSe film obtained by LMVR after 4 hours of reaction time. To the naked eye, the surface of such a sample is highly textured with open pores and appears pitch black. At a magnification of x 100 (Figure 3.3 a), the porosity is evident. The size of the pores permits full infiltration of the gel electrolyte incorporated in the cell. The nature of the interface thus formed plays a critical role in the performance of the cell. These porous electrodes will provide a large surface area and we expect therefore an excellent cell current flow and improved efficiencies. Scanning electron micrographs of the same sample at magnifications of x 2000 and x 5000 (Figures 3.3 b and c) reveal the topographical details of CdSe samples and give us a very good idea about the depth within the film. The surface appears granular at a magnification of x 2000 and these grains, which range in size from 5 to 7 μm, are aggregates of much smaller crystals.

Figure 3.4 b shows a SEM micrograph of a typical CdSe electrode made by electrodeposition on Ti (t = 60 min)[73]. At a magnification of x 3000,

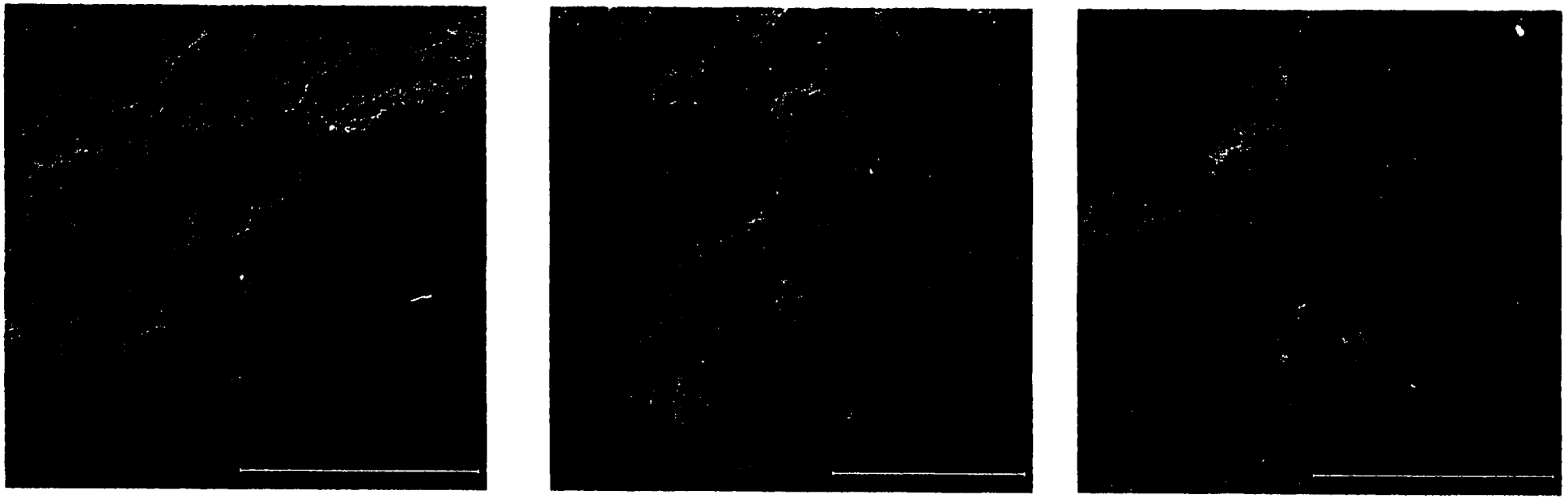

X 100 (a)

X 2000 (b)

X 5000 (c)

Fig. 3.3 SEM micrographs of CdSe films prepared by LMVR at different magnifications.

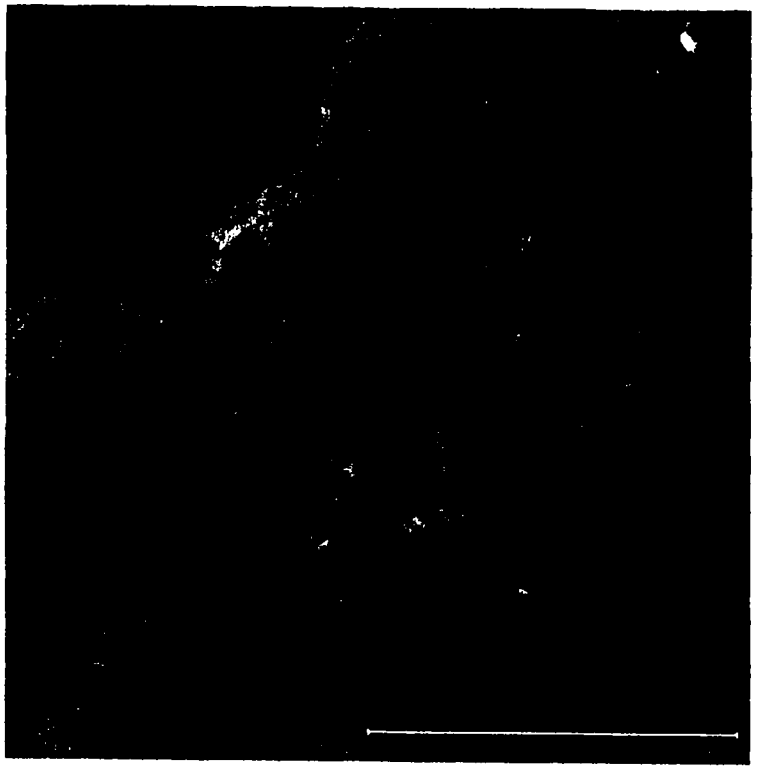

X 5000 (a)

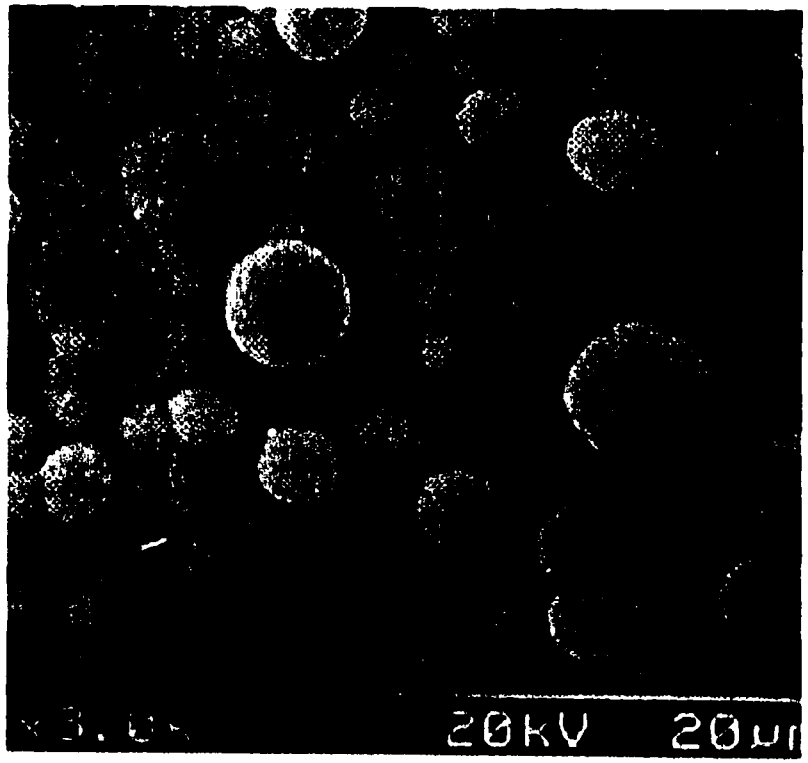

X 3000 (b)

Fig. 3.4 SEM micrographs of CdSe electrodes prepared by LMVR (a) and electrodeposition (b)[73].

the as-deposited films show an average size of the grains of 4-5 μm. As compared with the SEM micrograph of a CdSe electrode made by LMVR (x 5000; Figure 3.4 a), the structure shows a decrease in porosity and this will limit the real effective surface area of the semiconductor/electrolyte interface. Therefore, the light absorption and generation of the photocurrent are expected to be less efficient with these electrodes. We have seen that the efficiency of CdSe (ED)/gel electrolyte/ITO cells is low; an improvement would be to use CdSe electrodes made by LMVR despite the expected higher rate of recombination of photogenerated e^- - h^+ pairs.

3.3 Energy Dispersive Analysis of x-rays

Chemical composition of the CdSe thin films was determined by energy dispersive analysis of x-rays (EDAX). In the present study, a number of films prepared by LMVR were analyzed, and Cd:Se atomic ratios near 1.00 were occasionally found. However, most of the films had ratios greater than 1 (an average of 1.26 over 4 samples that were analyzed), indicating that the samples are richer in Cd. The atomic and weight percentages of two samples are given in Table 3.3. The excess in Cd may be due to the fact that the reaction proceeds by the diffusion of interstitial metal atoms through the chalcogenide thin film formed at the onset.[52,53] It is, therefore, possible that the percentage of Cd increases in going from the surface to the bulk of the sample, since Se only reacts with the Cd at the surface. Both methods, EDAX and x-ray diffraction, clearly demonstrate the presence of the Cd in the samples. A consequence of this chemical composition would be that the CdSe films are probably n-type semiconductors.

Table 3.3 Atomic and weight percentages of Cd and Se in two CdSe samples made by LMVR.

CdSe		Atomic %	Weight %
Sample 1	Cd	53.27	61.88
	Se	46.73	38.12
Sample 2	Cd	54.27	62.76
	Se	45.72	37.02

CHAPTER 4

ELECTROCHEMICAL MEASUREMENTS

4.1 Current-Voltage Characteristics in the Dark

We characterize a semiconductor as n- or p- type depending upon whether the conduction is due to electrons or holes, respectively. For II-VI semiconducting compounds, the conductivity type can be controlled by varying the stoechiometry of the semiconductor. For example, in CdSe an excess of cadmium acts as a donor and a non-stoechiometric film of CdSe rich in cadmium is observed to be n-type. The EDAX results, previously presented, established that n-CdSe films made by LMVR are richer in cadmium, therefore an n-type semiconducting behaviour is expected. It is also significant to correlate the EDAX results with the dark current-voltage (dark I-V) curves of thin film CdSe electrodes in contact with an electrolyte. These curves characterize the semiconductor/electrolyte junction that acts like a diode. The dark I-V curves of an n-type material should show a rectifying behaviour with a cathodic current much greater than the anodic current.

Dark current-voltage measurements are commonly used to analyze the electrical characteristics of photoelectrochemical cells because they provide an effective way to determine fundamental performance parameters such as rectifying behaviour, series resistance, shunt resistance, and diode saturation currents. A method that provides qualitative information concerning the rectifying behaviour of the cell is cyclic

voltammetry (CV). This technique uses a two-electrode system comprised of a working electrode and a counter electrode. The two electrodes are placed in electrical contact via an electrolyte solution. The measurements in this chapter were performed with an n-CdSe (LMVR) // gel electrolyte: PVDF (20%), (DMSO:DMF) (40:60), (1.34 M CsT:0.13 M T_2) //ITO cell like the one described in section 2.6 (Figure 2.2). The procedure used for dark I-V measurements on photoelectrochemical cells involves covering the cell to eliminate light-generated current. Then, a voltage is swept between two values (V_1 and V_2) at a fixed scan rate. When the voltage reaches V_2, the scan is reversed and the voltage is swept back to V_1.

The initial phase of our work was to determine if the solvent mixture (DMSO/DMF) could decompose and possibly contribute to the measured current. The working electrode in all cases is CdSe (LMVR); the counter electrode is Pt. For these experiments, the two electrodes were placed in a beaker containing 30 ml of liquid electrolyte with and without redox couple. For economic reasons, the less expensive redox couple HT/T_2 was used. Figure 4.1 illustrates I-V measurements in the dark at 25°C for DMSO/DMF (40/60) only (first scan) and for DMSO/DMF (40/60) with the redox couple HT/T_2 (1.34 M/0.13 M) (the second and the third scans). The exposed area of the working electrode was the same for each CV, so direct comparisons could be made. The parameters under which these results were carried out are: potential range from -1.5 V to 1.5 V and a scan rate of 1mV/s. As it is evident from Figure 4.1, the second and third scans exhibit currents higher than the first one. The current is enhanced by the presence of the redox couple HT/T_2 and the current produced by the DMSO/DMF mixture can be neglected, as it is practically zero.

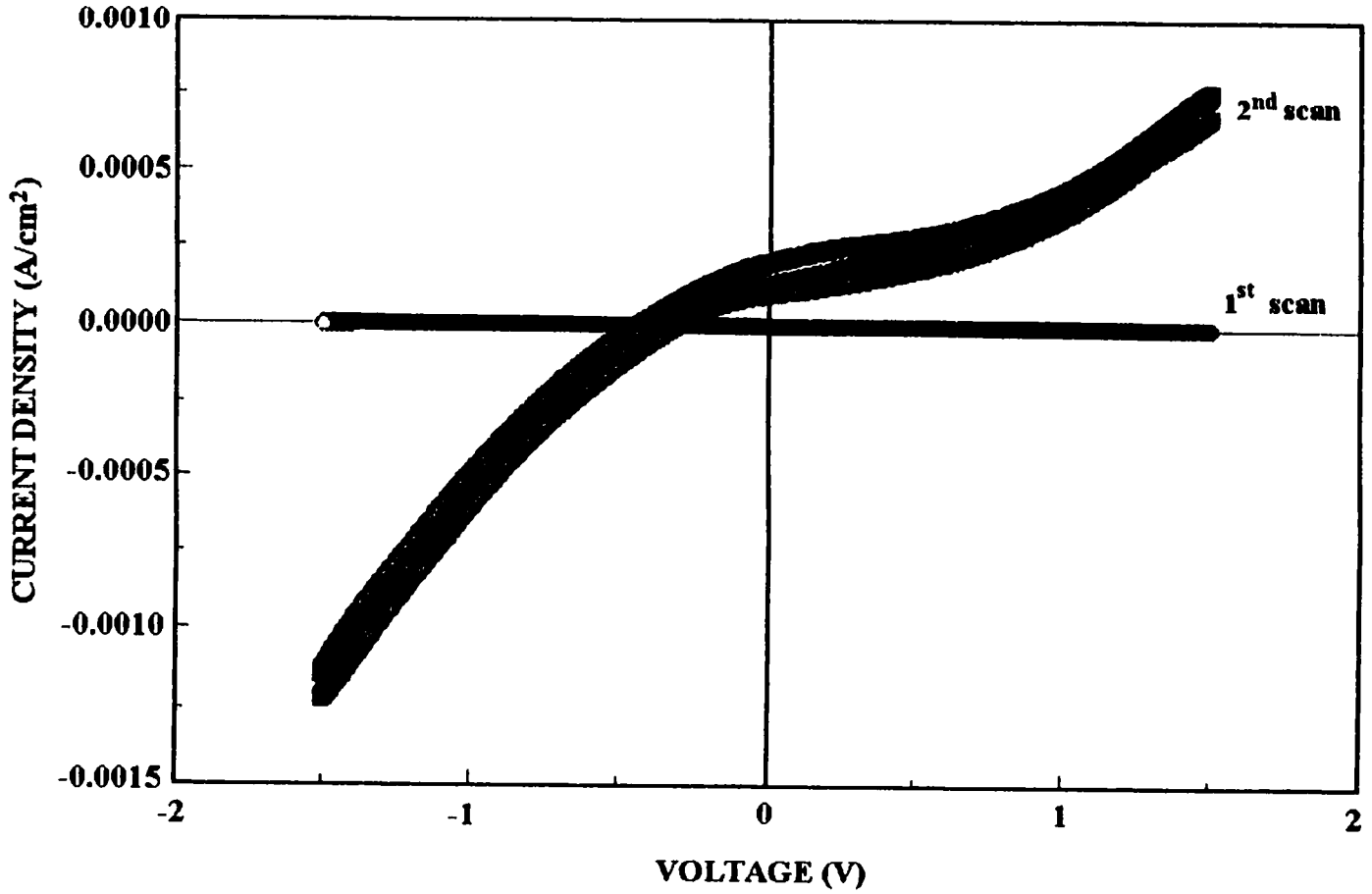

Fig. 4.1 I-V characteristics of the cells n-CdSe (LMVR)// (DMSO:DMF),(40:60)//Pt (first scan) and n-CdSe (LMVR)// (DMSO:DMF) (40:60), (1.34 M HT:0.13 M T_2)// Pt (second and third scan) in the dark. CdSe surface area: ~ 1 cm^2; potential range –1.5 to 1.5 V; scan rate: 1 mV/s; 3 cycles.

It is also obvious that the anodic dark current doesn't pass through zero, as expected. It should be emphasized that this behaviour is not observed for current–voltage measurements in the dark in a typical cell. We can only suggest two reasons that might give an explanation of why the anodic dark current doesn't pass through zero: (i) the Pt electrode that shows different kinetics from those of ITO, (ii) the distance between the working and the counter electrode (higher electrolyte resistance).

Having confirmed that the solvent mixture, DMSO/DMF has very little or no contribution to the measured current density, further tests were carried out to fully investigate the n-CdSe (LMVR) // gel electrolyte: PVDF (20%), (DMSO:DMF) (40:60), (1.34 M CsT:0.13 M T_2) //ITO cell in the dark. Figure 4.2 presents the I-V characteristics of the cell in the dark at room temperature. In order to determine the rectification ratio ($|i_c| / i_a$) for such a cell, the cathodic current (i_c) is measured at -1.45 V and the anodic current (i_a) is measured at +1.45 V. The conditions under which these curves were obtained are: (i) potential range from –1.5 to 1.5 V; (ii) potential scan 10 mV/s; (iii) three cycles. The faster scan rate (10 mV/s) will diminish the time for the experiment but will not affect the rectification ratio. The curves show that the cell behaves as a diode and the calculated rectification ratio is 7.4. The low value found for the rectification ratio for the cell investigated in this work suggest a not so good quality of the n-CdSe/gel electrolyte interface. The dryness of the gel electrolyte in contact with the CdSe electrode can be an important source of this behaviour. At room temperature, the gel is not warm anymore and it shrinks. As a consequence, the contact surface area diminishes and hence the cathodic current diminishes.

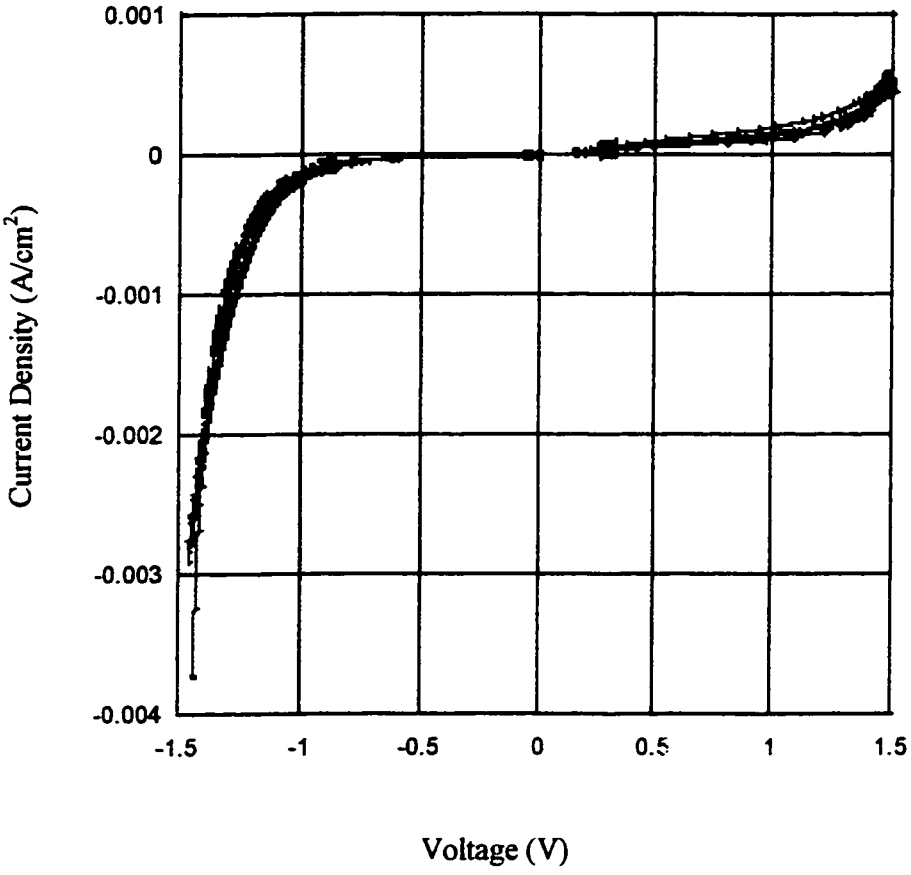

Fig. 4.2 I-V characteristics of the cell n-CdSe (LMVR)//PVDF(20%), (DMSO:DMF) (40:60), (1.34 M CsT :0.13 M T_2)// ITO in the dark for the determination of the rectification factor. CdSe surface area: 0.2 cm^2; potential range: –1.5 to 1.5 V; scan rate: 10 mV/s; 3 cycles.

The current-potential curve in the dark is described by the following equation[96]:

$$i = i_0 \left[\exp\left(\frac{\pm e(V - IR_s)}{nkT} \right) - 1 \right] + \frac{(V - IR_s)}{R_{sh}A} \qquad (4.1)$$

where i_0, I, *e*, *n*, *k*, R_s, R_{sh} *and A* represent, respectively, the exchange current density, the current (current density multiplied by the surface area), the electron charge, the Schottky diode quality factor, the Boltzmann constant, the cell series resistance, the cell shunt resistance and the surface area of the semiconductor/electrolyte interface. In equation 4.1, the plus sign refers to anodic currents (p-type semiconductor) and the minus sign to cathodic currents (n-type semiconductor). The determination of these parameters implies a detailed analysis of the curve from Figure 4.2. Parameters i_0, n, R_s and R_{sh} affect the photovoltaic conversion efficiency of the cell.

The cell shunt resistance is associated to the leakage current at the semiconductor grain boundaries or to fine electrolyte bridges along the microfissures.[82] The shunt resistance, whose value is ideally infinite, can be determined from the linear part of the current potential curve in the region of zero applied potential (Figure 4.3). In this case, the first term of equation 4.1 is negligible and R_{sh} is given by the inverse of the slope of the I-V curve. The high but not infinite calculated value of 1.4 MΩ may suggests that the CdSe (LMVR) / gel electrolyte junction is of a good quality but because the current-potential curve doesn't pass exactly through zero (but very close), the obtained value may not reflect the reality.

The cell cathodic current density may be represented by equation 4.2, for values of V more negative than –0.1V:

$$i = i_0 \left[\exp - \frac{e(V - IR_s)}{nkT} \right] \quad (4.2)$$

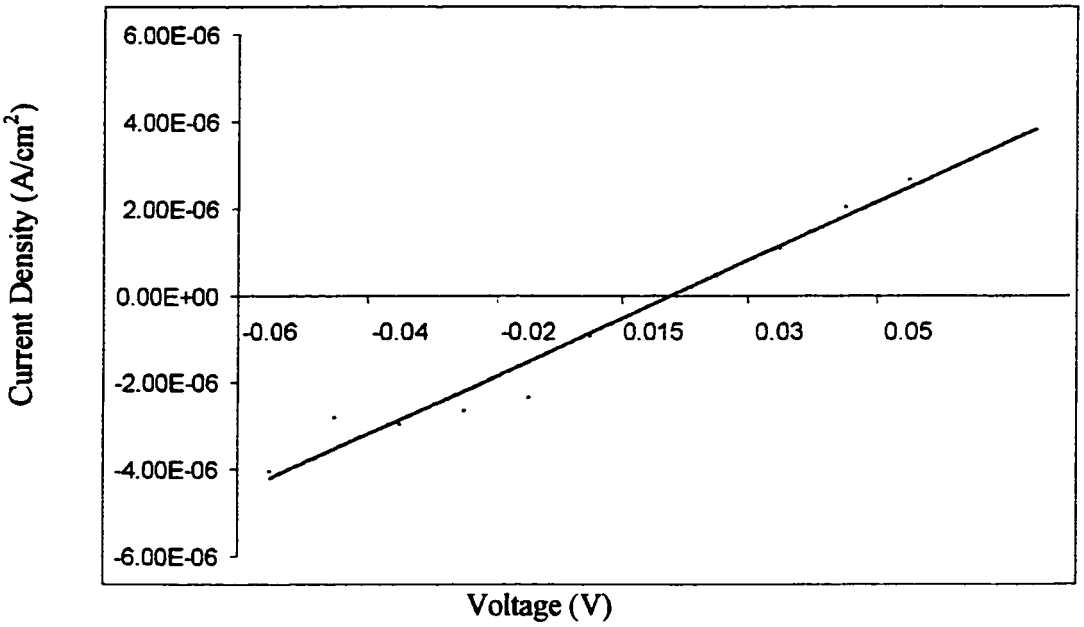

Fig. 4.3 Current potential curve near potential zero.

When I or R_s is very low, there exists a linear relationship between log |i| and |V| (Figure 4.4):

$$\log|i| = \log|i_0| + \frac{e|V|}{2.303\,nkT} \quad (4.3)$$

The calculation of the slope of the straight line allows the determination of the Schottky diode quality factor (n).

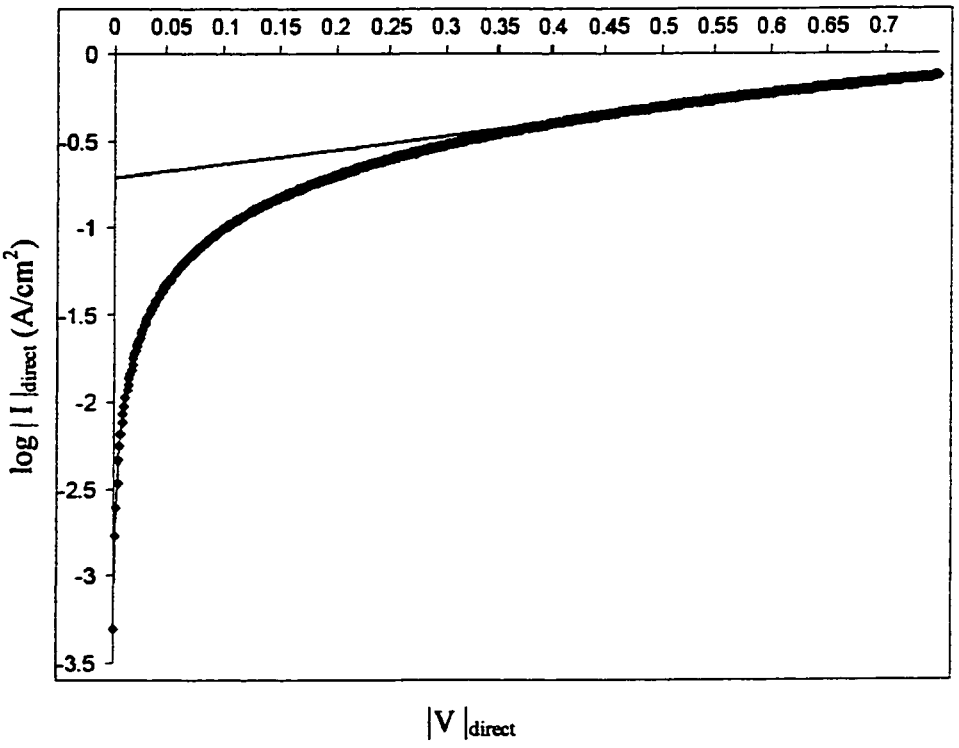

Fig. 4.4 Plot of log|i|$_{direct}$ versus |V |$_{direct}$ for the cell n-CdSe (LMVR) /gel electrolyte/ ITO studied in the dark.

For the cell investigated in this work n = 17. This value indicates that the n-CdSe/ gel electrolyte junction is far from being ideal, in which case n would be equal to 1. It is interesting that the n value of a polycrystalline semiconductor/electrolyte junction is higher than the n value of the corresponding single crystal semiconductor/electrolyte interface, and that the diode quality factor increases with the decrease of the crystallite size. [88] As shown in chapter 3, section 3.1, CdSe appears to be less crystalline than electrodeposited CdSe, and therefore the number of grain boundaries within the

polycrystal is increased. The consequence of this will be an increase in the recombination mechanism at grain boundaries and hence, a decrease of current density.

4.2 Current – Voltage Characteristics under the Light

The conversion efficiency (η) is defined as:

$$\eta = \frac{P_{max}}{P_{inc}} = \frac{V_{oc}\ i_{sc}\ ff}{P_{inc}} \tag{4.4}$$

and the fill factor (FF) is given by:

$$ff = \frac{P_{max}}{V_{oc}\ i_{sc}} = \frac{(Vi)_{max}}{V_{oc}\ i_{sc}} \tag{4.5}$$

with P_{inc} as the incident light power, V_{oc} as the open circuit voltage, I_{sc} as the short circuit current density, and i_{max} and V_{max} as the cell current density and voltage, respectively, at the cell maximum power : $P_{max} = (i\ V)_{max}$.

On the current-voltage curves, we identify the open-circuit voltage as the voltage across the illuminated cell at zero current, and the short-circuit current density as the current through the illuminated cell when the voltage across the cell is zero. The cell must be maintained at a constant temperature and a radiant source with a constant intensity must be used. For these experiments, a voltage is applied between 2 points ($V_1 = 0$, $i_1 = i_{sc}$) and ($V_2 = V_{oc}$, $i_2 = 0$). The parameters V_{oc} and I_{sc} can be directly determined from the curve and i_{max}, V_{max}, P_{max}, ff, and η are easily calculated.

Figure 4.5 presents the current-voltage curve of one of the more efficient n-CdSe (LMVR) // PVDF (20%), (DMSO:DMF) (40:60), (1.34 M CsT:0.13 M T_2) //ITO cells at room temperature, under white light illumination at an intensity of 30 mW/cm^2. The actual illuminated surface area is 0.2 cm^2. No correction has been done for visible light absorption by the ITO/polymer electrolyte interface. Direct comparison of the I-V curves under the light and in the dark for the same cell shows an increase of photocurrent with time.

A short-circuit photocurrent density of 1.3 mA/cm^2 and an open-circuit photovoltage of 0.63 V are observed with this cell. The value 1.3mA/cm^2 represents the density current under illumination from witch the density current in the dark wasn't subtracted. The shaded area of Figure 4.6 represents the maximum power that can be derived from the solar cell. V_{max} and i_{max} are the voltage and the current density at the maximum power 8.63 x 10^{-2} mW/cm^2.

Ideally, a solar cell should have $V_{max} = V_{oc}$ and $i_{max} = i_{sc}$. However, various loss mechanisms operating within the cell, such as bulk recombination and interface recombination of minority charge carriers make it deviate from the ideal behaviour. The term used to express this difference is known as the fill factor (ff), which equals 0.10 for this cell. The cell gave a photovoltaic conversion efficiency of $\eta = 0.27$ % as calculated according to equation 4.4.

A factor limiting the conversion efficiency of the cells is the low photovoltage.

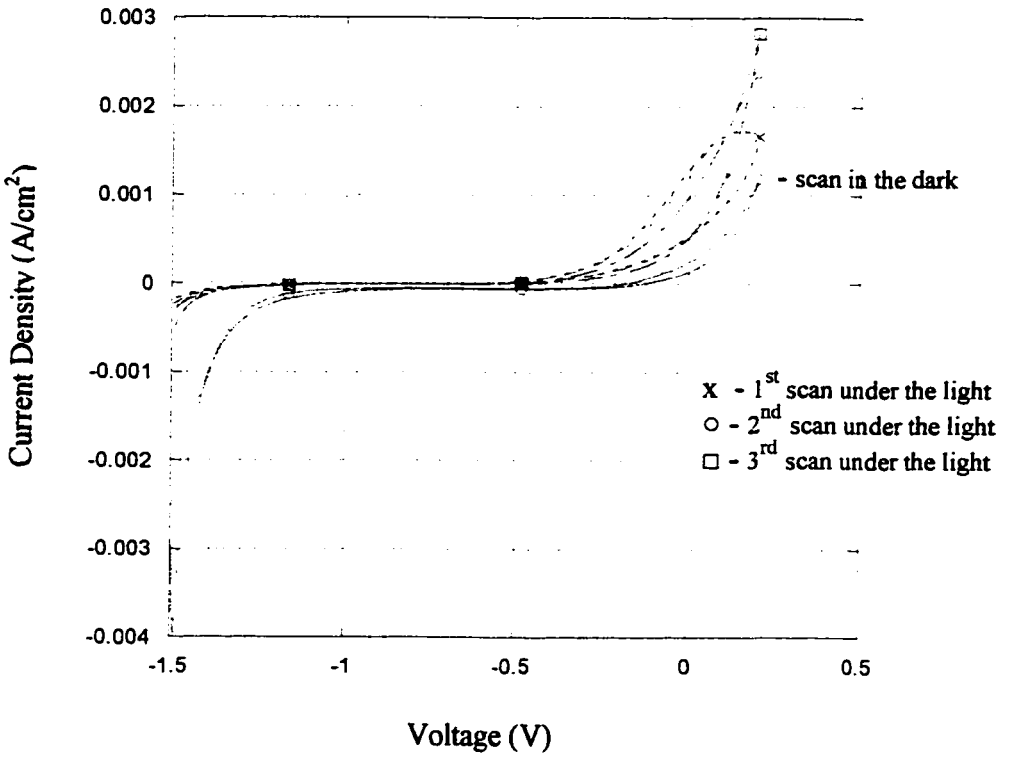

Fig. 4.5 Current voltage curves of the PEC n-CdSe (LMVR)//PVDF(20%), (DMSO:DMF) (40:60), (1.34 M CsT :0.13 M T_2)// ITO in the dark (__) and under illumination (.....) at 22^{0}C. CdSe surface area: 0.2 cm^2; power of the incident light (tungsten halogen lamp): 30 mW/cm^2; potential range: -1.5 to 0.2 V; scan rate: 10 mV/s; 3 cycles.

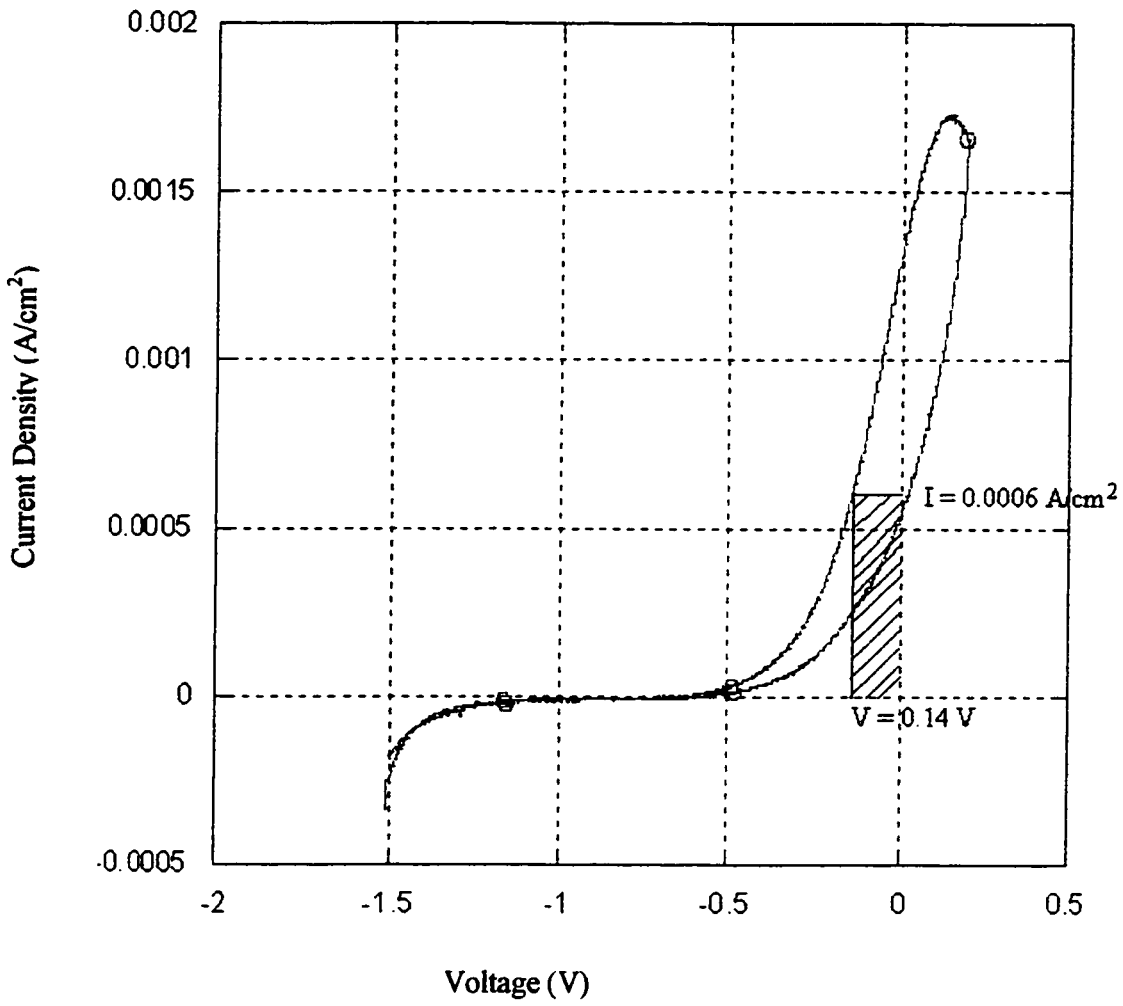

Fig. 4.6 The maximum power that can be derived from a solar cell n-CdSe (LMVR)//PVDF(20%), (DMSO:DMF) (40:60), (1.34 M CsT :0.13 M T_2)// ITO under illumination (____) at 22^{0}C. Cd Se surface area: 0.2 cm^2; power of the incident light (tungsten halogen lamp): 30 mW/cm^2; potential range: -1.5 to 0.2 V; scan rate: 10 mV/s.

Charge recombination at the electrode/ electrolyte junction usually plays a significant role in limiting the photovoltage and the photocurrent. From previous work, a significant increase in V_{oc} can be expected at higher light intensity. Figure 4.7 shows the current-voltage curves for a cell in the dark and under white light illumination at intensity of 100 mW/cm^2. This cell indicates a different performance in comparison with the cell illuminated at an intensity of 30 mW/cm^2. It can be seen that the open-circuit voltage (V_{oc}) increases progressively from 0.6 V to 0.86 V, but no increase of the short-circuit current density (i_{sc}) is observed with increasing of the light intensity (saturated value). The calculated fill factor (ff) for the cell illuminated at an intensity of 100 mW/cm^2 is 0.1. The low short-circuit currents and poor fill factors, as compared with solid-state photocells, can be caused by the slowness of the polysulfide (T_2) reduction at the cathode. The fact that I_{sc} is not increased with the light intensity is an indication that the transfer kinetics is not sufficiently rapid to accommodate the higher photon fluxes (diffusion-limited reaction). This can lead to very small photocurrents, limiting the power output. The substantial improvement in V_{oc}, however, results in a very small increase in the photovoltaic conversion efficiency: η = 0.3%. A major limitation to the conversion efficiency for these cells might come from the difficulty in achieving better kinetics at the counter electrode.

4.3 Spectral Response of CdSe Electrodes

The measurement of a solar cell photocurrent spectral dependence, usually referred to as the action spectrum, provides additional information on the device. An accurate photocurrent spectral response may be used to study the cell quantum yield, the minority

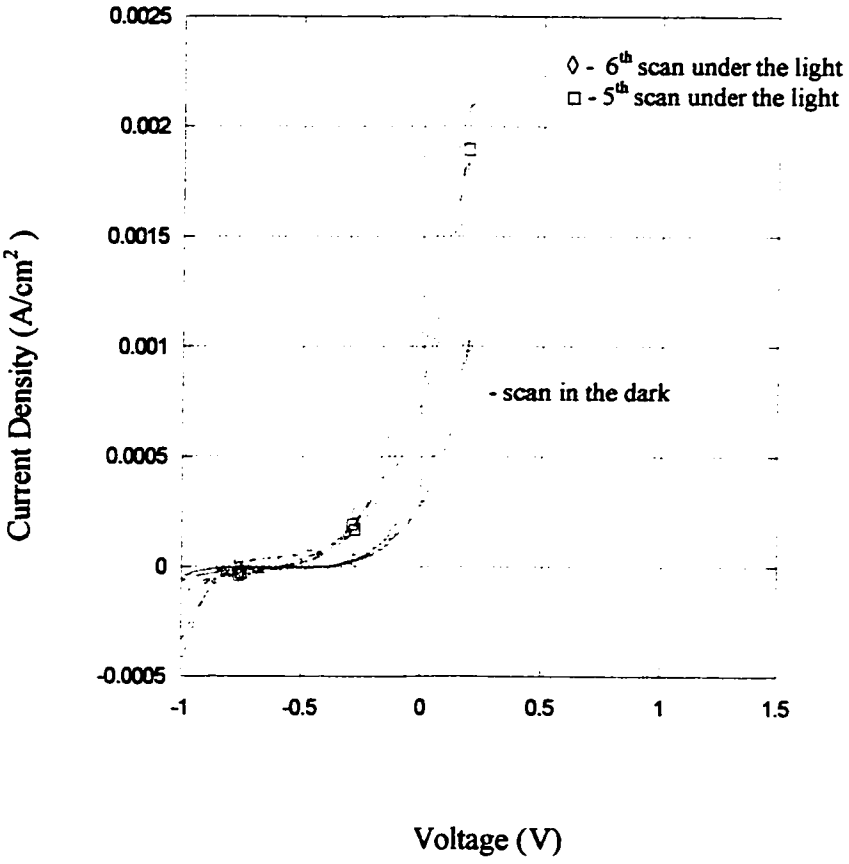

Fig. 4.7 Current voltage curves of the PEC, n-CdSe (LMVR)//PVDF(20%), (DMSO:DMF) (40:60), (1.34 M CsT:0.13 M T_2)// ITO in the dark (___) and under illumination (.....) at 22^0C. CdSe surface area: 0.2 cm^2; power of the incident light (tungsten halogen lamp): 100 mW/cm^2; potential range: -1 to 0.2 V; scan rate: 10 mV/s.

carrier diffusion length in the semiconductor and its band gap. The accuracy, however, is often reduced because of physical and practical limitations related to the low illumination levels provided by usual monochromatized light sources. The overall short-circuit current density spectral response of the photoelectrochemical cell using CdSe is shown in Figure 4.8. The short-circuit current was measured as a function of wavelength from 400 to 800 nm.

Two corrections have been done in determining the photocurrent response spectra.

1) The dark current was subtracted from the current under illumination.
2) Because the incident monochromatic light generated by the tungsten-halogen lamp has different intensities at different wavelengths, the photocurrents have been normalized for a constant photon flux.

The obtained spectrum is characterized by an increase in the photocurrent at 750 nm, which stabilizes at 430 nm.

Theoretically, for a direct gap material like CdSe, the absorption coefficient (α) near the absorption edge is described by[83,84]:

$$\alpha = \frac{A\,(h\nu - E_g)^{0.5}}{h\nu} \tag{4.6}$$

and the quantum efficiency at wavelength λ (Φ_λ) is given by[85]:

$$\Phi_\lambda = \frac{I_{sc,\lambda}}{qA\phi_{0,\lambda}} = 1 - \frac{EXP(-\alpha W)}{1 + \alpha L_p} \tag{4.7}$$

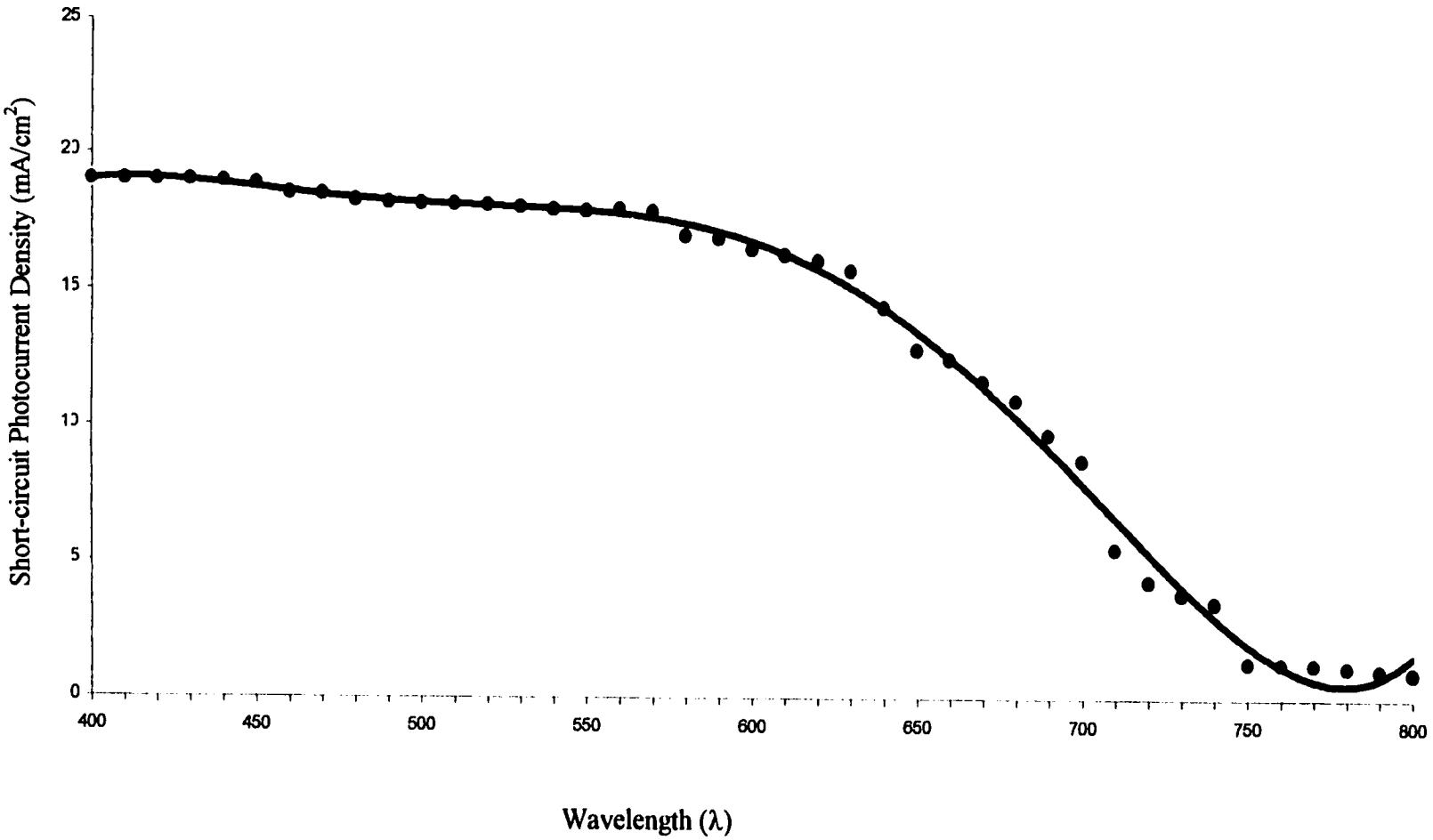

Figure 4.8 Spectral response of CdSe. PEC: n-CdSe (LMVR)//PVDF(20%), (DMSO:DMF) (40:60), (1.34 M CsT:0.13 M T_2)// ITO

where $I_{sc,\lambda}$ is the short-circuit photocurrent at wavelength λ, q is the electronic charge, A is the sample area, and $\Phi_{0\lambda}$ is the incident light flux at wavelength λ, W is the depletion layer width and L_p is the diffusion length for holes (minority carriers in n-type CdSe). Considering absorption coefficients such that $\alpha L_p << 1$ ($1 + \alpha L_p \approx 1$) and $\alpha W << 1$, expansion of equation (4.7) yields

$$\Phi_\lambda \approx \alpha (W + L_p) \tag{4.8}$$

Combining equations (4.6) and (4.8), a plot of $(I_{sc,\lambda} h\nu)^2$ *vs* $h\nu$ should give a straight line with intercept on the X-axis equal to the band gap energy. This plot is shown in Figure 4.9. The linear relationship indicates a direct band gap energy of 1.72 eV, which is in good agreement with the value of 1.74 eV reported in the literature for this material.[86] Departure from the straight line at low photon energy may be attributed to impurities or structure defects levels located within the material band gap.[87] Optical absorption studies demonstrate that CdSe made by electrodeposition method possesses a direct band energy of 1.75 eV which is also in good agreement with the value of 1.74 eV reported in literature.[68]

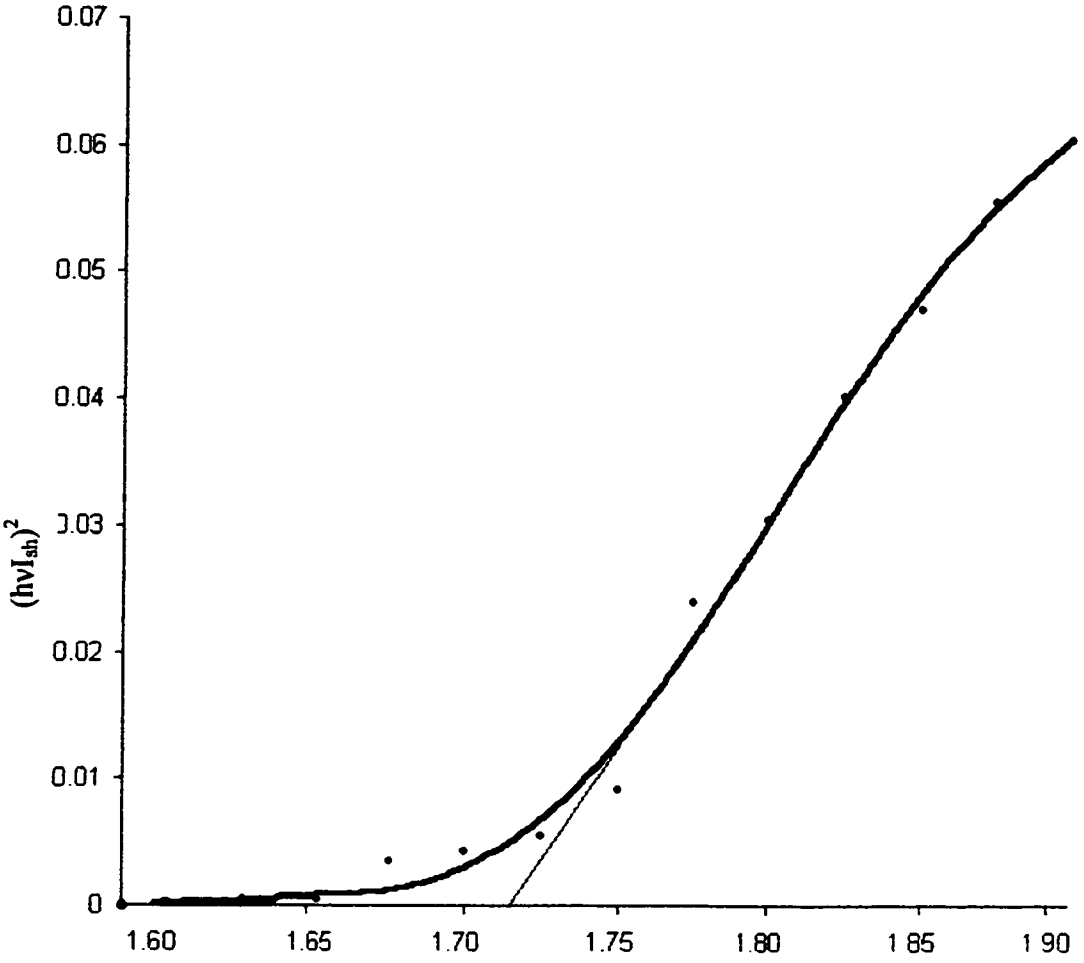

Fig.4.9 Plot of $(\alpha h\nu)^2$ versus photon energy for CdSe.
PEC: n-CdSe (LMVR)//PVDF(20%), (DMSO:DMF) (40:60), (1.34 M CsT:0.13 M T_2)// ITO

CHAPTER 5

CONCLUSION AND SUGGESTIONS

5.1 Conclusions

With a band gap energy of 1.72 eV, CdSe is an attractive candidate for a PEC cell for conversion of light into electricity using terrestrial solar irradiation. Therefore, in order to optimize the following type of electrochemical photovoltaic cell, n-CdSe/gel electrolyte/ ITO, it is important to simultaneously optimize the photoelectrode efficiency and electrolytic properties of the electrolyte. We started with a systematic investigation of the preparation of thin CdSe films by liquid metal vapour reaction. LMVR is an attractive and simple method for CdSe thin film preparation as indicated by a series of factors:

1) Preparation of CdSe at low temperature (330^0 C) prevents large deviations in the stoechiometry of the film.

2) The cadmium substrate provides a good ohmic contact since the CdSe layers are grown directly from the metal plate (1 mm thick).

3) It produces polycrystalline CdSe films with improved light-harvesting capability.

4) And of course, the advantage of low cost fabrication; including low temperature, no high power supply, high vacuum or expensive equipments.

The electrodes were characterized by x-ray diffraction, SEM, EDAX and cyclic voltammetry. For comparison, we also took into account the results of the analysis made for CdSe electrodes obtained by electrodeposition, reported by previous workers.

From x-ray analysis, it is observed that the CdSe electrodes prepared by the two methods might exhibit a mixture of hexagonal and cubic structures. The x-ray diffraction patterns suggest a hexagonal phase with a preferential orientation of the crystallites for the (110) and (112) planes in CdSe made by LMVR, while the hexagonal phase of the crystallites in CdSe made by electrodeposition shows a different orientation: (101), (102), (103) and (112) planes. In both cases, the position of the observed diffraction peaks corresponds reasonably well to those reported by JCPDS. The diffraction patterns show broad and less intense peaks in the case of CdSe made by LMVR and narrower and much intense peaks in the case of CdSe made by electrodeposition. This indicates that electrodeposition method produces CdSe electrodes with a better crystallinity than the electrodes made by LMVR, suggesting more significant $e^- - h^+$ recombination at the grain boundaries in a PEC under illumination The calculated hexagonal lattice parameters for CdSe made by LMVR (a = b = 4.3 Å, c = 6.98 Å, c/a = 1.63 Å) are close to those reported for electrodeposited CdSe: a = b = 4.28 Å, c = 6.99 Å, c/a = 1.63 Å[68] and in fairly good agreement with the literature values: a = b = 4.3 Å, c = 7.02 Å, c/a = 1.63Å.[79]

The morphological studies of CdSe made by LMVR show that the surface area of the electrodes is increased, with respect to that of electrodeposited electrodes, due to the columnar grains extending from the substrate up to the surface. The CdSe electrodes made by LMVR have a textured surface that was made naturally in the process of the

liquid metal-vapour reaction. This surface effect will contribute to the enhancement of short-circuit photocurrent values (i_{sc}). A short-circuit photocurrent density of 1.3 mA/cm^2 was found for n-CdSe (LMVR)//PVDF(20%), (DMSO:DMF) (40:60), (1.34 M CsT:0.13 M T_2)// ITO cell while for n-CdSe (electrodeposited)//PVDF(20%), (DMSO:DMF) (40:60), (1.34 M CsT:0.13 M T_2)// ITO cell, the short-circuit photocurrent density was 100 times smaller, 0.01 mA/cm^2.[73]

In the dark, the electrode/gel electrolyte interface shows a rectifying behaviour typical of a non-ideal Schottky junction (n = 17) between an n-type semiconductor and an electrolyte. Under white light illumination (area = 0.2 cm^2), at an incident intensity of 30 mW/cm^2, the cell exhibits the following characteristics: i_{sc} = 1.3 mA/cm^2, V = 0.63 V, ff = 0.10 and η = 0.27 %. Values of these parameters are higher than those reported for the electrodeposited CdSe/gel electrolyte/ITO cell: $i_{sc} = 1.1 \times 10^{-2}$ mA/cm^2, V_{oc} = 0.39 V, ff = 0.12, $\eta = 1.7 \times 10^{-3}$ %.[73] The higher short-circuit current in CdSe (LMVR)/gel electrolyte/ITO cell indicates that the method of preparing CdSe by LMVR for use in photoelectrochemical cells is promising since it can be used to prepare large area electrodes.

Semiconductor photoeffects in contact with a gel electrolyte are largely affected by properties such as the electrolyte redox potential, conductivity, viscosity, charge transfer kinetics at the interface, solution stability and transparency. Previous work and this work too, demonstrated that the highly positive potential of the CsT/T_2 redox couple (0.52V vs. NHE) leads to an increase in the open circuit voltage from 0.6V to 0.86V when the cell is illuminated with white light at an intensity of 100 mW/cm^2 instead of 30 mW/cm^2.

Optical absorption studies demonstrated that CdSe electrodes made by LMVR possesses a direct band gap energy of 1.72 eV, which is close to the value of 1.75 eV found for the electrodeposited CdSe electrodes[68] and that is in agreement with the literature value, 1.74 eV.[86]

5.2 Suggestions

For future studies:

1. There are many design options and the reliability of these designs can only be tested experimentally. This will form a major part of the next phase of work.
2. Chemical composition of the electrolyte is a particularly important parameter in PEC systems based on complex electrolytes. In the case of gel electrolytes, finding a molten redox couple that will eliminate the presence of the solvent can make a real improvement. The use of the solvent mixture DMSO/DMF (60/40) gives, in our case, the highly ionic conductivity of the gels. But, at the same time, it creates problems due to evaporation and drying of the gel.
3. Attempts should be made to improve the catalytic properties of the counter-electrode. An efficient photoelectrochemical conversion requires such a counter-electrode.

The stability of the cells has not been monitored for periods of time long enough for their consideration as practical solar energy converters. This may be further improved by taking into consideration the suggestions given above.

REFERENCES

1. A.L. Fahrenbruch and R.H. Bube, *Fundamentals of solar cells*", 1, (1983).
2. J. Roy, *M. Sc. Thesis*, Concordia Universiy, Montreal, Canada, (1979).
3. A.F Cuevas, R.A. Sinton, and R.R. King, *"Technology-based comparison between two-sided and back-contact silcon solar cells," in Proc. 10th Euro. Commun. Photovolt. Solar Energy Conf.* (Lisbonne, Portugal), April (1991).
4. R.A. Sinton, and R.M. Swanson, *"Design criteria for Si point-contact concentrator solar cells," IEEE Trans. Electron DeWces*, **ED-34,** 2116-2123 , (1987).
5. R.A Sinton, and R.M Swanson, *"Simplified backside-contact solar cells," 7hms. Mectron Devices*, **37**(2), 348-352, (1990).
6. R.A. Sinton, R.R. King, and R.M. Swanson, *"Novel implementations of backside-contact silicon solar cell designs in one-sun and concentrator applications", in Proc. of the 4th IREE Photovoltaic Science and Engineering Conference*, (Sydney, Australia), Feb. (1989).
7. RA. Sinton, *"Device physics and characterization of silicon point-contact solar cells", Ph.D. dissertation*, Elec. Eng. Dept., Stanford Univasity, Stanford, CA, 47-52, (1987).
8. P. Verlinden, B. Lafontaine, O. Evrard, E. Mazy, and A. Crahay, *"High-Efficiency backside contact solar cells with a self-aligned process and new texturization technique for silicon," in Proc. 10th Euro. Commun. Photovolt. Solar Energy Conf.* (Lisbonne, Portugal), April (1991).

9. T.L. Chu, S.S. Chu, R.W. Kelm, Jr., and G.W. Wakefield, *"Solar cells from zone-refined metallurgical silicon," J. Electrochem. Soc.: Solid State Science and Technology,* **125** (4), 595-597, (1978).

10. E. Becquerel, *Compt. Rend.*, **9**, 461 (1939).

11. W.G. Adams and R.E. Day, *Proc. Royal Soc.*, **A25**, 113 (1877)

12. C. Hu and R.M. White, *Solar Cells: From Basic to Advanced Systems*, (McGraw-Hill Inc., New York), **6** (1983).

13. H. Gerischer, *J. Electroanal. Chem.*, **82**, 133 (1977).

14. A.J. Bard and M.S. Wrighton, *J. Electrochem. Soc.*, **124**, 1708 (1977).

15. J.G. Mavroides, J.A. Kafalas, D.F. Kolesar, *Appl. Phys. Lett.* **28**, 241 (1976).

16. J.G. Mavroides, D.I. Tchernev, J.A. Kafalas, D.F. Kolesar, *Mater. Res. Bull.*, **10**, 1023 (1975).

17. H.Tributsch and J.C. Bennett, *J. Electroanal. Chem.*, **81**, 97 (1977).

18. B. O'Regan and M. Cratezet, *Nature*, **353**, 737 (1991).

19. Z. Deng, M. Cinquino and M.F. Lawrence, *J.Mater. Res.*, **6**(6), 1293 (1991).

20. J. Barthel, H.J.Gores and L. Kraml, *J. Phys. Chem.*, **100**, 1283, (1996).

21. M.Sharon, P. Veluchamy, C. Natarajan and D. Kumar, *Electrochim. Acta*, **36**, 1107 (1991).

22. B.A. Parkinson, A. Heller and B.Miller, *Appl. Phys. Lett.*, **36**, 521 (1978).

23. B.A. Parkinson, A. Heller and B.Miller, *J. Electroanal. Chem. Soc.*, **126**, 955 (1979).

24. G. Kline, K.Kam, D.Canfield and B.A. Parkinson, *Solar Energy Materials*, **4**, 301 (1981).

25. G. Kline, K.Kam, R. Ziegler and B.A. Parkinson, *Solar Energy Materials*, **6**, 337 (1982).

26. A. Heller, K.C. Chang and B.Miller, , *J. Electrochem. Soc.*, **124**, 697 (1977).

27. T.A. Skotheim, *Appl. Phys. Letter*, **38**, 712 (1981).

28. T.A. Skotheim, *J. Electrochem. Soc.*, **129**, 894 (1982).

29. T.A. Skotheim and O. Inganas, *J. Electrochem. Soc.*, **132** (9), 2116 (1985).

30. B.Marsan, D. Fauteux and A.K.Vijh, *Solid State ionics*, **28-30**, 1058 (1988).

31. A.K.Vijh and B.Marsan, *Bull. Electrochem.*, **5** (6), 456 (1989).

32. M.G. Mglin and C.A. Angell, *J. Phys. Chem.*, **95**, 9464 (1991).

33. J.-M. Philias, *M.Sc. Thesis*, Université du Québec à Montréal, Montréal (1995)

34. O. Bohnke, C. Rousselot, P.A. Gillet and C. Truche, *J. Electrochem. Soc.*, **139** (7), 1862 (1992).

35. G. Dautzenbergy, F. Croce, S. Passerini and B. Scrosati, *Chem. Mater.*, **6**, 538 (1994).

36. A. Reiche, T. Steurich, B. Sandner, P. Lobitz and G. Fleischer, *Electrochem. Acta*, **40** (13-14), 2153 (1995).

37. X. Sun, W. Lin and X. Jing, *J. European Polymer*, **32** (6), 801 (1996).

38. U. Park, Y. Houg and S. Moh, *Electrochem. Acta*, **41** (6), 849 (1996).

39. F. Lohmann, *Z. Naturforsch.*, **22A**, 843 (1967).

40. A.J. Nozik, *Ann Rev. Phys. Chem.*, **29**, 189 (1978).

41. M. Prince, *J.Appl. Phys.*, **26**, 534 !1955).

42. S. Licht, R. Tenne, J. Flaischer and J. Manassen, *J. Electrochem. Soc.*, **133**, 52 (1986).

43. G. Hodes, J.Manassen and D.Cahen, *Nature* (London), **261,** 403 (1976); *Bull. Isr. Phys Soc.*, **22**, 100 (1976).

44. A.B. Ellis, S.W. Kaiser and M.S. Wrighton, *J. Am. Chem. Soc.*, **98**, 1635, 6418, 6855 (1976).

45. B. Miller and A. Heller, *Nature* (London), **262**, 680 (1976).

46. H.C. Chang, A. Heller, B.Schwartz, S.Menezes and B.Miller, *Science*, **196**, 1097 (1977).

47. B. Miller, A. Heller, M.Robbins, S. Menezes, K.C. Chang and J. Thomson, Jr., *J. Electrochem. Soc.*, **124**, 1019 (1977).

48. B. Miller, J. Reichmann, H. Witzke, S.K. Deb, and S.N. Chen, J. Electrochem. Soc., 127,725 (1980)

49. R.Haak, D. Tench, and M. Russak, *J. Electrochem. Soc.* , **131**, 2709 (1984).

50. M. Tomkiewicz, I. Ling, and W.S. Parsons, *J. Electrochem. Soc.*, **129**, 2017 (1982).

51. H.O. Finklea, *Semiconductor Electrodes*, 1988.

52. D. Iwanov and C. Nanev, Acta Physica Academiae Scientiarum Hungaricae 47, 83 (1979).

53. J.S. Curran, R. Philippe, M.Roubin, and L. Mosoni, *Solar Energy mater.*, **9**, 329 (1983).

54. M.F. Lawrence, N. Du, R. Philippe, and J.P. Dodelet, *J. Cryst. Growth, **84**, 133 (1987).*

55. M.F. Lawrence, N. Du, G. Stremsdoerfer, R. Philippe, and J.P. Dodelet, *Electrochem. Soc. Ext. Abs.*, **86-1**, 467 (1986).

56. J. S. Curran, R. Philippe, and G. Stremsdoerfer, *J. Electroanal. Chem.*, **187**, 121 (1985).

57. G. Hodes, and J. Manassen, *J. Electrochem. Soc.*, **127**, 544 (1980).

58. S. Licht, R. Tenne, G. Dagan, G. Hodes, J. Manassen, and D. Cahen, *Appl. Phys. Lett.*, **46** (6), 608 (1985).

59. S. Licht, R. Tenne, H. Flaisher, and J. Manassen, , *J. Electrochem. Soc.*, **133**, 52 (1986).

60. S. Licht, *J. Phys. Chem.*, **90**, 1096 (1986).

61. S.J. Visco, and L.C. De Jonghe, *J. Electrochem. Soc.*, **135**, 2905 (1988).

62. S.J. Visco, C.C. Mailhe, L.C. De Jonghe, and M.B. Armand, *J. Electrochem. Soc.*, **136**, 661 (1989).

63. M. Liu, S.J. Visco, and L.C. De Jonghe, *J. Electrochem. Soc.*, **136**, 2570 (1989).

64. J. Shi, M. Malservisi, and B. Marsan, *Electrochim. Acta*, **40** (13-14), 2425 (1995).

65. S.J. Visco, M. Liu, M.B. Armand, and L.C. De Jonghe, *Mol. Cryst. Liq. Cryst.*, **190**, 185 (1990).

66. B. Marsan, *Ph.D. Thesis*, INRS-Energie, Université du Québec à Montréal, 1988.

67. B. Marsan, and M. Malservisi, *Electrochim. Acta*, **37** (9), 1645 (1992).

68. J.-M. Philias and B. Marsan, *Electrochim. Acta*.

69. I. Renard, *M. Sc. Thesis*, Université du Québec à Montréal, (1997).

70. J.W. Cho, and G.W. Lee, *J. Polymer Science part B – Polymer Phys.*,**34**, 1605 (1996).

71. J.P. Southall, A.M. Voice, V. Rogers, G.R. Davies, J.E. McIntyre, and I.M. Ward, *Seventh International Meeting on Lithium Batteries*, Boston, Massachusetts, USA, May 15-20, Poster I-B-26 (1994).

72. H. Li, I. Renard, and B. Marsan, *Abstracts, 191th Meeting of the Electrochemical Society*, Montréal, Québec, Canada, May 4-9, (1997).

73. Hongmei Li, Ph.D. Research Proposal, Concordia University,1998

74. A.M. Voice, J.P. Southall, V. Rogers, K.H. Matthews, G.R. Davies, J.E. McIntyre, and I.M. Ward, *Polymer*, 1996.

75. F. Croce, F. Gerace, G. Dautzemberg, S. Passerini, G.B. Appetecchi and B. Scrosati, *Electrochim. Acta*, **39**, 2187-2194 (1994).

76. H.S. Choe, J. Giaccai, M. Alamgir and K.M. Abraham, *Electrochim. Acta*, **40** (2289-2293) (1995).

77. B.D. Cullity, *Elements of X-ray diffraction 2nd ed.*, Addison-Wesley Publishing Company, Reading, 1978.

78. W.F. McClune, Powder diffraction file of inorganic phases, Standard #19-191, JCPDS international Center for diffraction Data, Swarthmore, 1979.

79. W.F. McClune, Powder diffraction file of inorganic phases, Standard #8-459, JCPDS international Center for diffraction Data, Swarthmore, 1979.

80. W.F. McClune, Powder diffraction file of inorganic phases, Standard #5-682, JCPDS international Center for diffraction Data, Swarthmore, 1979.

81. M. Bujatti, Proc. IEEE 53,397 (1965).

82. H. Hovel, in: A. Beer, R. Willardson (Eds.), Semiconductors and Semimetals, vol. 11, Academic Press, New York, 1975.

83. K. Colbow, D.J. Harrison, and B.L. Funt, *J. Electrochem. Soc.*, **128**, 547 (1981).

84. P.C. Searson, and L.M. Latanision, *J. Electrochem. Soc.*, **135**, 1358 (1988).

85. M.A. Butler, *J. Appl. Phys.*, **40**, 1914 (1977).

86. R.C. Weast, Handbook of Chemistry and Physics,55th ed.,CRC Press, Cleveland, 1974-1975, p. E-101.

87. E. Elizalde, F. Rueda, M.T. Gutierrez, J. Ortega, P. Savador, Solar Energy matter.13 (1986) 407.

88. K. Sen, B.P. Tyagi, J. Appl. Phys. **56** (1984) 1240.

89. Z. Deng, *M.Sc. Thesis*, Concordia University, Montreal, 1990.

90. A.J. Dekker, *Solid State Physiscs*, 1963, **313**.

91. K.L.Chopra and S.R. Das, *Thin Film Solar Cells*, 1983, **211**, **233**, **240**.

92. S. Licht, R. Tenne, H. Flaisher, and J. Manassen, *J. Electrochem. Soc.*, 1986, **52**.

93. *ibid*, Standard # 7782-49-2 (1995).

94. *ibid*, Standard # 7440-43-9 (1995).

95. W.F. McClune, *Powder diffraction file of inorganic phases*, Standard # 5-682, JCPDS International Center for Diffraction Data, Swarthmore, 1979.

96. J.-M. Philias, and . B. Marsan, *Electrochim. Acta*,.44, 2915 (1999).